ANL-7441

Argonne National Laboratory

CRYSTAL STRUCTURES OF CUBIC AND TRIGONAL YTTRIUM HYPOCARBIDES; A DIMORPHICALLY INTERPHASED SINGLE-CRYSTAL STUDY

by

M. Atoji and M. Kikuchi

The facilities of Argonne National Laboratory are owned by the United States Government. Under the terms of a contract (W-31-109-Eng-38) between the U. S. Atomic Energy Commission, Argonne Universities Association and The University of Chicago, the University employs the staff and operates the Laboratory in accordance with policies and programs formulated, approved and reviewed by the Association.

MEMBERS OF ARGONNE UNIVERSITIES ASSOCIATION

The University of Arizona	Kansas State University	The Ohio State University
Carnegie-Mellon University	The University of Kansas	Ohio University
Case Western Reserve University	Loyola University	The Pennsylvania State University
The University of Chicago	Marquette University	Purdue University
University of Cincinnati	Michigan State University	Saint Louis University
Illinois Institute of Technology	The University of Michigan	Southern Illinois University
University of Illinois	University of Minnesota	University of Texas
Indiana University	University of Missouri	Washington University
Iowa State University	Northwestern University	Wayne State University
The University of Iowa	University of Notre Dame	The University of Wisconsin

Printed in the United States of America
Available from
Clearinghouse for Federal Scientific and Technical Information
National Bureau of Standards, U. S. Department of Commerce
Springfield, Virginia 22151
Price: Printed Copy $3.00; Microfiche $0.65

ANL-7441
Chemistry

ARGONNE NATIONAL LABORATORY
9700 South Cass Avenue
Argonne, Illinois 60439

CRYSTAL STRUCTURES OF CUBIC AND TRIGONAL YTTRIUM HYPOCARBIDES; A DIMORPHICALLY INTERPHASED SINGLE-CRYSTAL STUDY

by

M. Atoji and M. Kikuchi

Chemistry Division

May 1968

TABLE OF CONTENTS

TABLE OF CONTENTS

LIST OF FIGURES

LIST OF TABLES

CRYSTAL STRUCTURES OF CUBIC AND TRIGONAL YTTRIUM HYPOCARBIDES; A DIMORPHICALLY INTERPHASED SINGLE-CRYSTAL STUDY

by

M. Atoji and M. Kikuchi

ABSTRACT

The first single-crystal structure determination in the rare-earth and related carbides is presented here for yttrium hypocarbide, which exhibits two modifications: the high-temperature-disordered cubic structure having the composition YC_x ($x \cong 0.25$-0.65), and the low-temperature-ordered trigonal structure with the Y_2C stoichiometry. Both X-ray single-crystal and neutron powder techniques were employed in the structure determination.

Our quenched single crystal has stabilized the transient state in the midst of the cubic-to-trigonal transition, and consists of one cubic and four trigonal crystals with the trigonal triad axis parallel to one of four cubic triad axes. The domain sizes of these five crystals are different from one another, resulting in highly complex diffraction patterns for which exceedingly elaborate dimensional and intensity interpretations have been carried out. The chemical compositions of the sample crystal were determined accurately by means of the diffraction-intensity analysis. Several new statistical and analytical methods have been derived and incorporated in this work.

Our cubic structure, $YC_{0.48}$, has been uniquely determined to be a NaCl-type with $a = 5.115 \pm 0.002$ Å and with the carbon atom sites randomly occupied. The trigonal Y_2C shows an anti-$CdCl_2$-type configuration with $a = 3.617 \pm 0.002$ and $c = 17.96 \pm 0.01$ Å. The carbon atoms are located at the nonparameter positions, and the Y atoms are found at the one-parameter coordinates with $z = 0.2585 \pm 0.0003$. The Debye temperatures obtained from the isotropic temperature factors are 230 ± 10, 170 ± 5, and 233 ± 6°K for $YC_{0.28}$ (cubic), $YC_{0.48}$ (cubic), and Y_2C (trigonal), respectively.

The cubic-to-trigonal transformation is characterized by a slight yttrium-layer displacement along the triad axis and a migration of the carbon atoms to constitute a full and vacant layer sequence. Our multidomained single-crystal structure demonstrates an illuminating example of interphase and isophase boundary intercorrelation. Revelation of such interphased structure is also the first example in this type of compound.

The cubic YC_x structure has previously been postulated and the trigonal Ho_2C structure has also been reported, both through the powder technique. Our study has confirmed these results unambiguously and presents the structure parameters with a substantially higher accuracy, hence providing detailed insight into the chemical bonding and the phase-transition mechanism. A review of the related structures is given to emphasize striking differences in the bond properties between the rare-earth and transition metal carbides. The crystal structure of Sc_2C, previously reported incorrectly as having a cubic superlattice, has been proved here to be isostructural to the trigonal Y_2C.

I. INTRODUCTION

The course of this study spans nearly one decade, though quite intermittently, during which we have gone through somewhat confusing steps in reaching the ultimate goal: the crystal structure determination of yttrium hypocarbide, YC_x ($x \cong 0.25$-0.65). Independently, a French group (Dean et al., 1964; Bacchella et al., 1966; Lallement, 1966) was working on several other rare-earth hypocarbides, but their approach was not straightforward either. As described later in detail, a major cause for the confusion in our case arises from the fact that the rare-earth hypocarbide forms two closely related, yet different, crystallographic modifications which frequently coexist through intricate phase-boundary interrelations. In fact, our "single crystal" was composed of five single-crystal domains with mutually correlative axial relations. A detailed chronicle of bewildering successions in our prolonged endeavors is outlined in Ch. II, since it would be more than just instructive to disciplines in crystallographic research. Chapter II is written very much unmathematically in contrast to the following sections.

Both X-ray and neutron diffraction techniques were employed in the structure determination. We started with the powder diffraction method, for the single crystal was not then available. Later, accidentally, quite a few good single crystals were found in an arc-melted sample. These crystals were too small for neutron diffractometry, but just right in size for the X-ray experiment. The single-crystal X-ray diffraction patterns were, however, unusually complex. Nevertheless, we have obtained an unambiguous solution with which the neutron powder data were successfully interpreted. Detailed procedures of the structure analysis and the results are described in Chs. III through VI, where rather perplexed descriptions in Ch. II are straightened out with a strong emphasis on mathematical and numerical aspects.

The resultant structure has revealed not only some intriguing chemical bonding schemes but also has led to the suggestion of a sophisticated mechanism associated with an order-disorder behavior of the carbon atoms. In Ch. VII, these characteristics are discussed and the structures of the related compounds reviewed.

The dimorphic structures of yttrium hypocarbide to which we have referred are as follows: the NaCl-type cubic phase with a deficiency in the carbon atom sites as represented by YC_x ($x \cong 0.25$-0.65);* the trigonal (or rhombohedral) phase with the ordered carbon atoms leading to the chemical formula Y_2C. When we discuss yttrium hypocarbide in general or a mixed phase consisting of these two different structures, we use a generalized symbol YC_x. The cubic phase is frequently denoted by YC_x (cubic) or by "the cubic YC_x," whereas the trigonal phase is represented by Y_2C, implying a structurally definable carbon content. Also, we employ the terminology "cubic superlattice," which refers to the cubic structure having the unit-cell length twice that of the cubic YC_x.

The crystal structure of scandium hypocarbide has recently been reported to have an ordered, superstructure NaCl-type cubic configuration (Rassaerts et al., 1967). However, their X-ray powder data are more reasonably interpretable in terms of the trigonal Y_2C-type structure. Our proposed structure is described in the Appendix.

This work was initiated as a part of our crystal- and magnetic-structure studies of metal carbides. So far, the following results have been reported: the crystal structures of CaC_2, YC_2, LaC_2, LuC_2, and La_2C_3, all at room temperature; the crystal structures and paramagnetic scattering analyses at room temperature of YbC_2, Ce_2C_3, Pr_2C_3, and Tb_2C_3; the crystal and magnetic structures of CeC_2, NdC_2, PrC_2, TbC_2, HoC_2, DyC_2, and UC_2 in the range from room to liquid-helium temperatures. Among those cited above, by means of neutron diffraction, the magnetic spin alignment has been found in CeC_2, NdC_2, PrC_2, TbC_2, HoC_2, and DyC_2 at low temperatures, and their spin structures have subsequently been determined. Publications related to these subjects are listed in the References.

In all of the carbides mentioned above, the carbon atoms are dimerized, so that the structure consists of the metal atoms and C_2 molecules. The neutron crystal-structure analyses have revealed some interesting systematic relations among the interatomic distances. A simple, yet typical, example is that the intramolecular C-C distance becomes longer as the metallic valence increases. The neutron magnetic analysis has harvested a variety of new information: for example an abnormal valence state of Yb in YbC_2 and of Ce in Ce_2C_3; the crystal-field effects upon magnetically active electronic levels; strong anisotropic exchange interactions in the magnetic spin alignment.

We have been extending our program to the carbides containing interstitial-type carbon atoms so as to provide further data about metallic carbides, of which this report is an example. An elaboration of some topics

*This structure was proposed by the discoverer of this compound, Spedding et al., 1958.

is included in Ch. VII. It should be noted here that Lallement (1966) has carried out an extensive magnetic-susceptibility study on REC_x.*

Recently, low-temperature neutron experiments have revealed the existence of magnetically ordered phases in ErC_2, Tb_2C_3, Ho_2C_3, and the hypocarbide of Tb. Here, the Tb hypocarbide is isostructural to YC_x. Both the crystal- and magnetic-structure analyses of TbC_x have been hampered because only powder diffraction data have been available. This difficulty no longer exists, for the crystal structures of YC_x have uniquely been determined as reported here. The results of TbC_x will be published in due course.

The statistical errors of the measured quantities in this report are expressed in terms of the standard deviation unless otherwise noted.

*The symbol RE is used to indicate rare earth.

II. CHRONICLE OF STUDIES

A. Ames Period (1958-1960)

About 1955-1957 at Iowa State University, Ames, K. Gschneidner, Jr., under the supervision of F. H. Spedding and A. H. Daane, was working on his thesis subject, the rare-earth and carbon system. Their study (Spedding et al., 1958) revealed, among other new observations, the existence of the hypocarbides of yttrium and of the heavy rare earths from Sm to Lu, all of which are frequently represented here by REC_x. Since x had a value in the vicinity of 1/3, Gschneidner called them the tri-rare-earth carbide. Our terminology, hypocarbide, is due to Lallement (1966). Some authors employ "subcarbide" for the same. Our generalization includes yttrium among the "rare earths."

Spedding et al. (1958) have reported that the X-ray powder diffraction data of these hypocarbides could be reasonably interpreted on the basis of a face-centered cubic lattice of the rare-earth atoms. The X-ray scattering powder of carbon is much smaller than those of rare earths. Nonetheless, the X-ray powder analysis on the hypocarbide of the lightest metal in the series, YC_x, could distinguish whether the carbon atoms occupy the octahedral or tetrahedral interstitial holes in the yttrium matrix. It turned out that the former case is strongly favored. Hence, the resulting structure is of the NaCl type with randomly distributed vacancies in the carbon atom sites, or simply another Hägg's carbide. However, Gschneidner's photographs had a number of very weak extra reflections which were assumed to be due to some unknown impurities. These extra reflections very likely originated from the coexisting trigonal Y_2C, as described later.

For locating the carbon atoms, the neutron diffraction technique offers a powerful tool, since the neutron scattering amplitude of carbon is comparative to those of rare earths. The neutron diffraction studies of the rare-earth carbides including YC_x and TbC_x were then initiated. With the samples provided by Daane and Gschneidner, Atoji, then also at Iowa State, made several brief visits to Argonne and Oak Ridge during 1958-1959 for carrying out neutron experiments at these National Laboratories.

The neutron powder patterns of the rare-earth hypocarbides clearly exhibited several prominent extra reflections, some of which appeared to be indexable by doubling the X-ray cubic unit-cell dimension. The neutron patterns were of low resolution, and the overlapped peaks were resolved by means of a rather elaborate curve-fitting technique (Atoji, 1961; Atoji and Williams, 1961). A set of observed data was then subjected to numerous trial structures. Symmetries of the trial models covered from cubic down to triclinic by placing the carbon atoms in various ordered or disordered manners. None of the models rendered a completely satisfactory agreement with the observed data. The reason is now clear. The observed pattern is

composed of both the cubic and trigonal reflections (see Ch. VI), whereas all the trial analyses were carried out on the assumption that a single phase existed.

B. Argonne Trial Period (1960-1965)

The program moved from Iowa State to Argonne in 1960 following the transfer of Atoji, who had been actively involved in the construction of an automatic neutron diffractometer, particularly during 1960-1962. Nevertheless, about a dozen additional single-phase models were examined, with emphases on the cubic, trigonal, and hexagonal configurations. A cubic model which seemed to give the best agreement was reported at the Villanova Conference of the American Crystallographic Association (Atoji, 1962a). This model cannot be correct because of the single-phase assumption, but it happened to be very much identical to the reported structure of Sc_2C published in 1967 (see Appendix for our reinterpretation on the Sc_2C data).

In early 1963, an X-ray diffraction unit was acquired. Also, the new neutron diffractometer, with a high peak resolution, was readily available.

Consequently, complete rework on YC_x and TbC_x was initiated, using both X-ray and neutron methods. The samples were freshly prepared by J. L. Moriarty of the Lunex Company. Firstly, the X-ray powder photographs of the Lunex TbC_x were taken. The X-ray powder lines were markedly spotty, suggesting of fair-sized single-crystal grains in the Lunex arc-melted buttons.

At about this time, Yves Jeannin was visiting Argonne from France. Jeannin and Atoji selected a small sample piece from the crushed TbC_x button and inserted it into a thin-walled pyrex capillary. The capillary was then mounted on an X-ray precession camera, and the diffraction pattern was examined to see whether or not a good single crystal had been obtained. The process was patiently repeated. More than a score of the capillaries were made, and nearly a hundred of the lining-up diffraction patterns were taken. About a dozen single crystals large enough for the X-ray method were found. However, all gave blurred diffraction spots, implying large internal strains. Thermal annealing could not relieve the crystals from strains.

This stage lasted nearly two months (May-July, 1963). It seemed that a refined, improved powder method would be the best approach. Jeannin finished his visiting assignment around this time, and D. Tressider started to assist the program.

Consequently, the neutron powder diffraction patterns of YC_x and TbC_x were taken again, using the high-resolution diffractometer. Also, just for checking the purity, the Lunex YC_x was examined by the X-ray method.

Surprisingly, the very first X-ray sample happened to be a good strain-free single crystal (Oct 1963). It was subsequently found that the Lunex YC_x buttons are full of good single crystals having a size almost ideal for the X-ray technique.

A single crystal of YC_x having approximately cylindrical shape was selected and aligned on a precession camera. Strong reflections employed for lining up the crystal clearly indicated a cubic symmetry, and the measured lattice constant was in good agreement with Gschneidner's value (Spedding et al., 1958). Then a set of diffraction photographs for several principal reciprocal-lattice zones were taken with different time exposures.

The long-exposure films showed a number of weak additional reflections which appear to lie midway between the strong reflections, so that the NaCl-type cubic cell dimensions should be doubled in all directions. However, the intensities of these additional reflections exhibited a much lower symmetry than cubic. We shall tentatively call these weak superlattice-like reflections "noncubic reflections".

So as to determine the symmetry associated with the noncubic reflections, the experiment was extended to other zones. Even with a very long exposure, the noncubic reflections were still weak in intensity. For some zones, they exhibited certain pseudosymmetries, such as a mirror plane, with a few violating reflections. For some other zones, there is hardly any symmetry at all. Hence, the symmetry of the noncubic reflections appeared to be as low as triclinic. Consequently, almost all accessible zones including the higher reciprocal-lattice levels were carefully examined using the precession-camera technique. This complete survey experiment took nearly three months (Nov 1963 to Jan 1964).

Diffraction-intensity measurements were made at least twice for each reflection on different occasions. The number of individual visual measurements was as many as 9,000. The resultant intensity values were then intercorrelated using a statistical averaging technique. A final set of intensity data was thus obtained.

Around this time, an attempt was made to obtain more precise lattice constants. The measurements involved the distances among the diffraction spots. Astonishingly enough, it was found that some noncubic reflections did not lie exactly at the midpoint between the strong cubic reflections. The shift from the cubic superlattice position is very small but is detectable under careful observation.

It was then clear that to find the cause of this irregularity the measurement had to be carried out on these small shifts, both in its magnitude and direction. However, it was not an easy task to locate the centroid or fiducial edges of those weak noncubic reflections.

An optical densitometer was used to see whether precise measurement could be carried out. The densitometer trace was of disastrously poor quality because of low signal-to-noise ratio. A traveling microscope was also tried out; similar difficulty was encountered. Eventually, it was found that a staged, low-magnification comparator was best suited for this purpose. The strong cubic reflections were used as the fiducial points in measuring the shift magnitude.

The magnitude of the shift to be measured was in the range from 0.02 to 0.7 mm, and systematic correlations among the shifting modes could be made only when the accuracy of the measurement was better than about ±0.05 mm. Estimated maximum error in the individual visual measurement was as large as ±0.3 mm. Hence, there was no choice but to make as many measurements as possible in order to decrease the statistical error. Painstaking measuring work was then pursued. Approximately six measurements on one specific distance were carried out on different occasions. More than one thousand measurements were made.

In the interim, the Lorenz-polarization correction and the interzone correlations on the observed intensities were being carried out using the program written by H. G. Norment (1962). In the calculation of the Lorenz-polarization factor, the noncubic reflections were assumed to be at the cubic superlattice points. The shifts are so small that the error caused by this approximation is by no means significant.

There laid another high hurdle to conquer. The computer program contained a major error when applied to the precession case. Communications were exchanged between Norment and Atoji regarding this matter. A presumably amended program was sent to Argonne from J. Karle of Naval Research Laboratory. Norment had made further corrections. J. Gvildys of Argonne's Applied Mathematics Division helped with reprogramming. Finally, the correct computation was completed around July 1964 after a few months of struggling.

In parallel to this program, the neutron diffraction studies of other rare-earth carbides and related compounds were actively pursued. Because the problems on YC_x seemed unattractively complicated and because other problems were offering more exciting results, interest in the YC_x problem began to fade. Nevertheless, the intention of completing the subject matter was never discarded.

In the latter part of 1964, C. P. Kempter of Los Alamos Scientific Laboratory called Atoji and asked about the progress on YC_x and TbC_x. Also, Kempter stated that a French group had just published a paper on the structure determination on RE_2C (Dean et al., 1964) which yet could not explain the powder X-ray pattern obtained at Los Alamos. Now, the Argonne

group became aware that there were at least three groups working on essentially the same subject. The Argonne group was, however, the only one who had access to the single-crystal data.

This competition did stimulate the Argonne activity. During 1965, a considerable effort was made to find systematic relations among the shifting modes of the noncubic reflections. The distance measurements were repeated from time to time so as to improve the accuracy. Finally, a relation was found and was included in a discussion of the generalized reciprocal lattice (Atoji and Gvildys, 1966). At that time, the shifting characteristics were thought to be caused by a stacking disorder or the satellitic effect of an antiphase domain structure.

In the meantime, the French group corrected their own error in the structure determination of Ho_2C by doubling one of the unit-cell dimensions (Lallement, 1966). The positions of the carbon atoms were determined by means of neutron diffraction (Bacchella et al., 1966). The resultant structure is an ordered structure having a trigonal symmetry. All of the French results were entirely based on the powder data.

The Argonne group had suspected that this structure might still be incorrect, since the single-crystal patterns did not confirm the French results in the earlier stage of our interpretation. However, our final structure of Y_2C obtained from the single-crystal data turned out to be essentially a reconfirmation of the French result that was deduced from the powder data alone. Fortunately, as described later, our study has yielded a number of additional, unique structural informations with substantially higher accuracy.

C. Argonne Final Period (1966-1967)

Kikuchi started working on this subject in 1966. Still retained was a presumption that both cubic and noncubic reflections are originated from one crystal. Firstly, the small shifts of the noncubic reflections were neglected, and it was intended to include them in a refining process. Along this direction, all conceivable models were again tried out more systematically. The indices were converted to the hexagonal and rhombohedral symmetries to see whether or not some accidental extinctions observed in certain zones give some hint as regards the structure interpretation. This approach led to no place. In fact, the accidental extinctions mentioned above were frequently found to contradict one another. Also, possibilities of stacking faults and the antiphase domain structure were examined more thoroughly than before. A few months passed by without any conclusion.

When the intensity measurement was being carried out in 1963, it was noticed that the size of the diffraction spot of the noncubic reflection is somewhat smaller than the strong cubic spot. Therefore, it was always

in our mind that the noncubic reflections might have originated from a crystal different from that producing the cubic reflections. Certain twinning models were tried out, but not very thoroughly. Also, it was thought that the smaller sizes of the noncubic reflections may be due to the fact that these reflections are slightly off from the reciprocal plane containing the strong cubic reflections. This interpretation was also futile in its results. It then became obvious that the interpretation should have to start from the shifting-mode analysis which had thus far been stubbornly avoided. Subsequently, it was decided to undertake the shifting-mode analysis more intensively.

Subsequently, a number of additional interreflection distances were repeatedly measured and also those measured previously were re-examined. Various statistical treatments were tried to find possible systematic modes among the measured shift values.

In April 1967, a systematic relation was finally found in the shift-vector maps. A detailed account of this is given in Ch. V.A. Eventually, it became clear that our "single crystal" is composed of one cubic crystal and four trigonal crystals with definite intercrystal axial relations. The subsequent structure analysis was relatively straightforward, and its details are given in Chs. IV through VI.

III. EXPERIMENTAL

The sample was prepared by arc-melting a compressed mixture of 99.9% pure yttrium metal filings and powdered spectroscopic graphite electrodes. The mixing ratio was 95.69 and 4.31 w/o for yttrium and carbon, respectively, corresponding to the chemical formula Y_3C. The product is brassy metallic and is so brittle that it can readily be crushed into powders. It decomposes slowly in moist air, liberating various hydrocarbon gases. Although the decomposition rate of YC_x is much slower than that of CaC_2, all preparatory and handling procedures were carried out in a very dry, inert-gas atmosphere.

The chemical analysis of arc-melted buttons gave 94.0 ± 0.2 and 4.9 ± 0.1% for Y and total C, respectively. The free carbon was less than 0.1%. The method of Frazer and Holzmann (1960) was incorporated in the micro determination of carbon. The spectroscopic analysis revealed the following impurities, in %: Al, 0.08; Ti, 0.041; Er, 0.03; Cu, 0.02; Na, 0.02; all other metallic impurities, 0.03%. Some of these impurities apparently came in during the sample preparation and would be too small a quantity to play a significant role in our subject matter. To recapitulate, the final product as a bulk may be represented by $YC_{0.39}$ or $Y_{2.6}C$.

Single crystals mined out from the arc-melted buttons were examined by the X-ray precession-camera technique. The size of the crystal selected was approximately a cylinder, 0.17 mm in diameter and 0.22 mm in length. The cylindrical axis was nearly parallel to the $[1\bar{1}0]$ axis of YC_x (cubic).

Precession photographs were taken with the use of MoKα radiation. The $[1\bar{1}0]$ axis of YC_x (cubic) was set parallel to the spindle or horizontal axis of the precession camera. A precession angle of 30° was used mostly, but smaller angles, 25 and 21°, were also employed so as to enhance the intensities of certain reflections, utilizing different angular dependencies of the Lorenz-polarization factor. Successive, timed exposures were made of each zone. Because of an extensive intensity range to be measured, the typical time exposures were 0.25, 0.5, 1, 2, 4, 8, 16, 24, 32 and 48 hr.

Intensities were estimated visually with the aid of standard, timed scales prepared from single-crystal reflections using the sample crystal. The intensity range measured was as wide as 1 to 1000 in a relative scale. By means of Norment's computer program (1962), Lorenz and polarization factors were applied, and the structure factors were thus obtained.

The absorption correction to the precession data (Burbank and Knox, 1962) and the spreading and splitting effects of the diffraction spot due to the $K\alpha_1$ and $K\alpha_2$ components happened to be very much reciprocal to each other. Hence, no absorption correction was applied. Also, no significant extinction effect, both primary and secondary, was detectable.

The experimental procedure in the neutron case is described in Ch. VI.

IV. ANALYSIS ON CUBIC YC_x

A. NaCl-type Model

As mentioned in Ch. II, our "single crystal" diffraction pattern consisted of the cubic and trigonal reflections. The structure analysis of the cubic crystal is very elementary. Despite this, we shall present the analytical procedure in considerable detail, since it is based on the first single-crystal data ever obtained in the cubic rare-earth carbides.

Let us assume a NaCl-type structure for the cubic YC_x. We assume that the carbon atoms are randomly absent so that the structure factor is obtained by multiplying the carbon contribution by an occupancy factor x. Hence, the NaCl-type structure factor per unit cell for YC_x (cubic) is simply given by

$$F = 4(f_Y \pm x f_C), \tag{1}$$

where f_Y and f_C are the X-ray scattering amplitudes of yttrium and carbon, respectively; the positive and negative signs are taken when the $(hk\ell)$ indices are all even and all odd, respectively.

The observed and calculated structure factors are intercorrelated by

$$KF_{obs} = F \exp\left\{-B\left(\frac{\sin\theta}{\lambda}\right)^2\right\} = F_{calc}, \tag{2}$$

where K is the scale factor and the exponential function is the Debye-Waller temperature factor.

The least-squares refinement using the logarithmic conversion of Eq. (2),

$$\ell n\,(F/F_{obs}) = \ell n\, K + B\left(\frac{\sin\theta}{\lambda}\right)^2, \tag{3}$$

was carried out for determining the best values for K and B at a given carbon occupancy parameter x. The observed structure factor, F_{obs}, was obtained from a weighted average of at least a dozen independent measurements. The calculated structure factors were computed using the Hartree atomic scattering factors (Cromer et al., 1963), which are listed in Table I.

An overall statistical discrepancy between F_{obs} and F_{calc} is measured either by

$$R_1 = \sum w|KF_{obs} - F_{calc}| \Big/ \sum wK|F_{obs}| \tag{4}$$

or by

$$R_2 = \sum w(KF_{obs} - F_{calc})^2 \Big/ \sum wK^2F_{obs}^2. \qquad (5)$$

The latter is employed preferably here because of its direct relation to the least-squares residuals.

TABLE I. Observed and Calculated Structure Factors per Unit Cell for the Cubic $YC_{0.48}$. The calculated values for the case where the carbon atoms are placed randomly at the octahedral interstices are designated as "NaCl model," and those with the carbon atoms randomly at the tetrahedral interstices are denoted as "CaF_2 model." The standard deviations on the observed data are given. The atomic scattering factors employed are listed so as to facilitate our discussion in the text.

Indices	F_{calc} (NaCl model)	F_{calc} (CaF_2 model)	F_{obs}	f_Y	f_C
111	113.1	112.0	113.3 ± 4.8	31.47	3.84
200	120.0	107.8	125.9 ± 2.5	30.36	3.47
220	99.3	99.3	97.3 ± 2.1	26.99	2.59
311	80.7	84.2	81.3 ± 2.2	25.10	2.24
222	84.5	77.8	82.2 ± 3.2	24.58	2.15
400	74.0	74.0	77.2 ± 2.5	22.97	1.94
331	60.3	62.8	62.3 ± 1.2	21.97	1.84
420	63.3	58.5	61.3 ± 2.2	21.70	1.81
422	55.8	55.8	59.3 ± 1.3	20.55	1.71
511	47.3	49.2	46.0 ± 1.1	19.84	1.66
333	47.3	49.2	48.0 ± 2.4	19.84	1.66
440	44.4	44.4	47.3 ± 1.1	18.83	1.59
531	37.8	39.4	38.0 ± 0.6	18.30	1.57
600	40.0	36.9	42.3 ± 2.1	18.19	1.56
442	40.0	36.9	39.0 ± 1.1	18.19	1.56
620	35.8	35.8	34.0 ± 1.3	17.47	1.52
533	30.6	31.9	32.5 ± 1.1	17.07	1.50
622	32.2	29.7	34.0 ± 0.9	16.87	1.49
444	29.2	29.2	26.2 ± 1.0	16.38	1.46
711	24.7	25.8	21.6 ± 0.8	15.90	1.44
551	24.7	25.8	24.3 ± 0.7	15.90	1.44
640	26.2	24.1	28.0 ± 1.6	15.81	1.43
642	23.7	23.7	25.2 ± 1.9	15.34	1.41
553	20.1	21.1	22.3 ± 0.9	14.97	1.39
820	17.5	16.0	20.1 ± 1.1	13.99	1.32
644	17.5	16.0	18.3 ± 3.2	13.99	1.32

A plot of R_2 as a function of x is nearly a parabola having a minimum at x = 0.44, for which B = 1.97 Å^2. This curve is shown in Fig. 1 as ALL REFLECTIONS case. However, at low scattering angles, the overlapping effect of the ℓ = 2n trigonal reflections is small yet appreciable. The geometrical analysis suggested that the intensities of the first six reflections given in Fig. 2 and Table I were slightly overestimated owing to the overlapping. When these six reflections were discarded in the analysis, the R_2 minimum occurs at x = 0.48, with B = 1.85 Å^2. The curve labeled

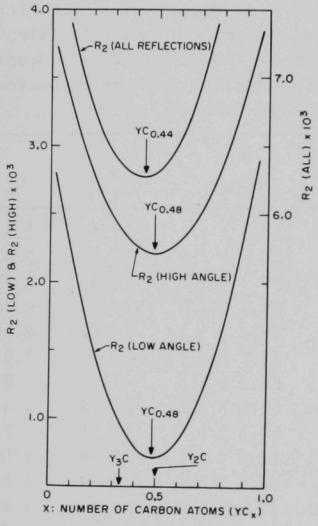

121-2695

Fig. 1

Determination of the Carbon Occupancy Parameter x in the Cubic YC_x. The discrepancy factors R_2 obtained from the least-squares refinement are plotted against various x values. The R_2 (LOW ANGLE) curve is obtained from the first six reflections in order of decreasing scattering angle, since the intensities of these reflections are slightly overestimated due to inclusion of the overlapping, weak trigonal reflections. All but these first six reflections are free from the trigonal reflections and lead to the R_2 (HIGH ANGLE) curve. For the R_2 (ALL REFLECTIONS) curve, the LOW and HIGH cases are treated as a whole.

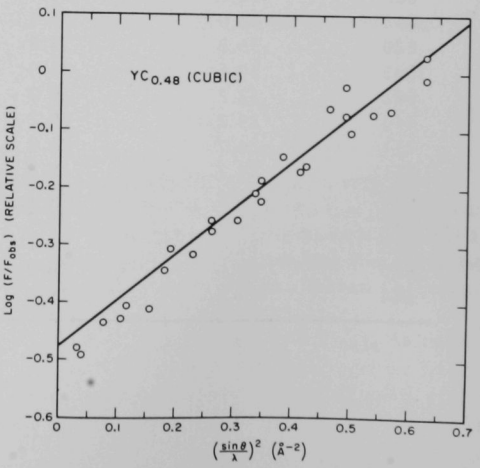

121-2686 Rev. 1

Fig. 2

A Graphical Representation of Eq. (3). Solid line is obtained from the least-squares parameters for the HIGH ANGLE reflections of $YC_{0.48}$ (cubic) (see Fig. 1). Note that the first six reflections with $(\sin\theta/\lambda)^2$ smaller than 0.175 Å^{-2} lie consistently below the solid line. This is due to small contributions from the overlapped ℓ = 2n trigonal reflections.

as HIGH ANGLE in Fig. 1 represents this case. The R_2 curve for the first six reflections is given in Fig. 1 as LOW ANGLE case. These LOW ANGLE values, x = 0.48 and B = 1.67 Å^2, are almost identical to the HIGH ANGLE case except for the different scale factor. The minimum discrepancy factors are R_1 = 7.5, 4.4, and 2.1%, and R_2 = 0.63, 0.22 and 0.072%, for ALL REFLECTIONS, HIGH ANGLE, and LOW ANGLE cases, respectively. In this sequence, the ratios among the scale factors are 0.950, 1.000, and 0.942.

An example of the least-squares fitting is shown in Fig. 2. The relative intensity contribution of the overlapping trigonal reflections was found to be nearly the same in all of the first six reflections. This manifests itself in the LOW ANGLE and ALL REFLECTIONS parameters being very closely equal to those for the HIGH ANGLE case (except for the differences in the scale factor).

The best set of parameters thus obtained are x = 0.48, giving the formula $YC_{0.48}$ and B = 1.85 Å^2. No strong evidence as regards the difference in the thermal parameters of Y and C was detected. The final values of F_{calc} and F_{obs} are listed in Table I, where the data for the first six reflections were obtained using the best parameters for the LOW ANGLE case, and the remainders were computed using the HIGH ANGLE parameters.

B. Other Models

Let us now compare the NaCl model with the CaF_2 model, the latter of which places the carbon atoms in the tetrahedral interstices of the yttrium matrix. We call the NaCl and CaF_2 models the octahedral and tetrahedral cases, respectively. The least-squares results for the tetrahedral case are also tabulated in Table I. The overall discrepancy factors for the tetrahedral case are R_1 = 5.7% and R_2 = 0.44%, whereas for the octahedral model R_1 = 3.7% and R_2 = 0.15%. The discrepancy factor favors the octahedral case, but this is hardly conclusive. This small difference between the two models is due obviously to a small scattering amplitude of carbon in comparison with the yttrium scattering amplitude (see Table I).

A firm support for the octahedral model could be found through the analysis given below. For a reflection with h odd, k odd, and ℓ odd, the difference between the structure factor per unit cell of the octahedral model and that of the tetrahedral model is equal to $-4xf_C$. Hence, we have

$$\sum \left\{ F_{calc}(\text{octahedral}) - F_{calc}(\text{tetrahedral}) \right\} = \sum (-4xf_C) = -120, \qquad (6)$$

where the summation is carried out over the all-odd index reflections in Table I excluding the first six reflections. Now,

$$\sum \left\{ F_{obs} - F_{calc}(\text{octahedral}) \right\} = 1 \cong 0, \tag{7}$$

which indicates almost complete agreement on the basis of the octahedral assumption. On the other hand,

$$\sum \left\{ F_{obs} - F_{calc}(\text{tetrahedral}) \right\} = -118, \tag{8}$$

which is essentially equal to -120 of Eq. (6), lending strong support to the octahedral model.

We extend this type of calculation to the reflections with ($h = 4n+2$, $k = 4n+2$, $\ell = 4n+2$), those with ($h = 4n+2$, $k = 4n$, $\ell = 4n$), and their equivalent reflections. For these reflections, we have

$$\sum \left\{ F_{calc}(\text{octahedral}) - F_{calc}(\text{tetrahedral}) \right\} = \sum 8xf_C = 144. \tag{9}$$

This is now compared with

$$\sum \left\{ F_{obs} - F_{calc}(\text{octahedral}) \right\} = 4 \cong 0 \tag{10}$$

and

$$\sum \left\{ F_{obs} - F_{calc}(\text{tetrahedral}) \right\} = 145. \tag{11}$$

Again, an excellent endorsement of the octahedral case results. The octahedral and tetrahedral models are indistinguishable for the reflection types ($h = 4n$, $k = 4n$, $\ell = 4n$) and ($h = 4n$, $k = 4n+2$, $\ell = 4n+2$). In this category,

$$\sum \left\{ F_{obs} - F_{calc}(\text{octahedral}) \right\} = \sum \left\{ F_{obs} - F_{calc}(\text{tetrahedral}) \right\} = 33. \tag{12}$$

The ideal value for Eq. (12) is zero and the observed small value can well substantiate this.

Similarly, other probable models, ordered or disordered in the carbon distributions, could be discarded as well, thus conclusively affirming the NaCl-type structure for the cubic YC_x.

V. ANALYSIS ON TRIGONAL STRUCTURE

A. Multiple Domain Structure

In order to facilitate the description, we have employed the terminology "trigonal" prematurely in many occasions. Needless to say, in order to establish the crystal symmetry, one has to determine not only the geometry of the crystal lattice, but also the symmetry in the diffraction intensity distribution. The latter comes in much later in this chapter, but the "trigonal" term has been and will appear frequently before the final symmetry determination.

Three typical precession photographs are given in Figs. 3(a), 4(a), and 5(a). Their explanatory diagrams are shown in Figs. 3(b), 4(b), and 5(b), where small displacements of the trigonal reflections from the cubic superlattice points are represented figuratively by means of arrows which we frequently call the shift vectors.

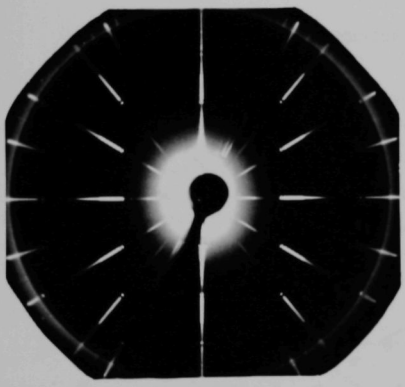

Fig. 3(a)

Precession Photograph (zero-level) of the Cubic [h, k, -(h + k/2)] Reciprocal-lattice Plane. Both the cubic and trigonal diffraction spots are seen here, but the latter spots are hardly visible. All trigonal reflections here are originated from the Type IV domain (Ref. Fig. 7).

121-2621

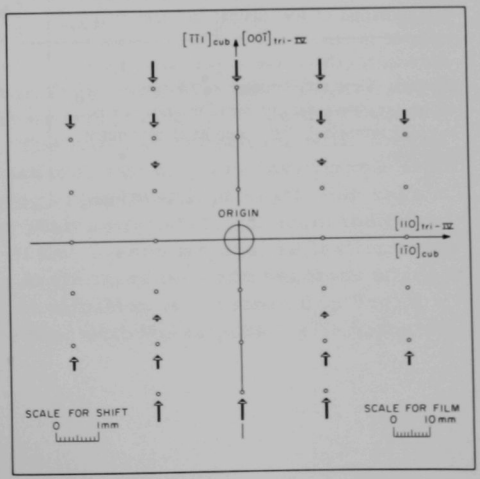

Fig. 3(b)

Explanatory Diagram for Fig. 3(a). Small circles represent the cubic reflections. Pertinent principal axes of the cubic and trigonal systems are shown. Arrows point out the directions of the shift of the trigonal reflections from the points corresponding to the cubic superlattice. The length of an arrow is proportional to the amount of the shift and is enlarged ten times the distance scaled for the cubic reflection pattern. The fiducial scales are given accordingly. The arrow with shaded tip and shaded shaft represents the shift vector of the Type IV domain. Also, the trigonal reflections with ℓ odd are our concern here, since those with ℓ even are overlapped with the cubic reflections or are too weak to give reliable data.

121-2689

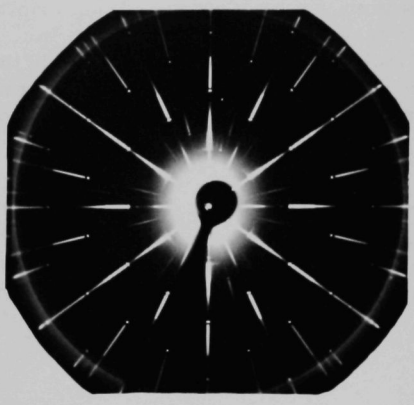

Fig. 4(a)

Precession Photograph (zero-level) of the Cubic ($hh\bar{\ell}$) Plane Showing Both the Cubic and Trigonal Reflections. The cubic reflections are generally stronger in intensity and larger in size in comparison with the trigonal reflections.

121-2620

Fig. 4(b)

Explanatory Diagram for Fig. 4(a). The trigonal reflections belonging to the Type II and III domains appear here. Shaded arrows represent the shifting modes of the Type II domain and open arrows are for the Type III domain. The trigonal reflections with ℓ odd are treated here. The notations A-1, A-2, ..., B-1, B-2, ..., $L(\bar{1}11)_{cub}$, and $(00\bar{3})_{tri}$ are given in conjunction with the lattice-constant determination of the trigonal structure as illustrated in Figs. 8 and 9. The shift-vector distribution exhibits two twofold axial symmetries. However, because of different domain size, the intensity distribution shows no twofold symmetry, but a center of symmetry (see text).

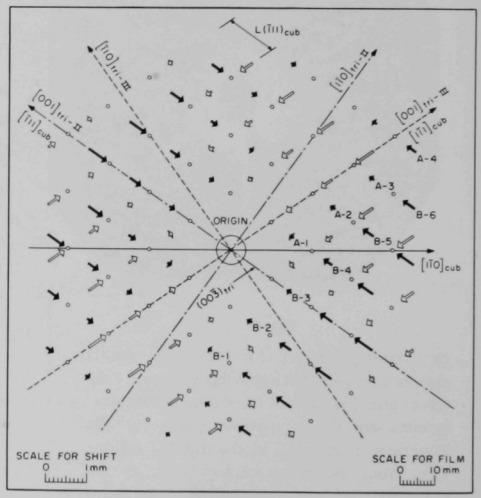

121-2687 Rev. 1

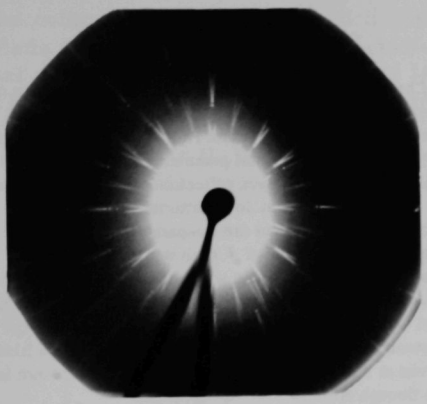

Fig. 5(a)

Precession Photograph (upper-level) of the Zone Corresponding to the (h, k, -1/2) Reciprocal-lattice Plane of the Cubic Phase. Here, no cubic reflections appear and the diffraction spots originate from all four trigonal crystals. Also, all trigonal reflections observed here should satisfy ℓ odd in (hkℓ).

121-2622

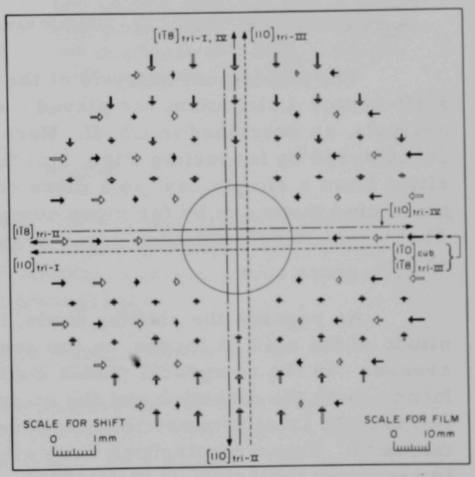

Fig. 5(b)

Explanatory Diagram for Fig. 5(a). The shading scheme of arrows belonging to the domains II, III, and IV are explained in Figs. 3(b) and 4(b). An arrow for the Type I domain is shown as a bottom-shaded arrowhead with open shaft. A large circle encompassing the origin confines a blind region, where no reflections are recorded owing to the geometrical screening-out in the upper-level precession setting.

121-2688

The vector diagrams shown in Figs. 3(b), 4(b), and 5(b) are for the trigonal reflections with ℓ odd in their indices (hkℓ), since they do not overlap with the cubic reflections. The trigonal reflections with ℓ even appear very close to the cubic reflections, and they are inseparable from the cubic reflections at low scattering angles. At high scattering angles, the trigonal reflections with ℓ even start to separate out from the cubic reflection. However, the intensity of the ℓ-even trigonal reflection fades away very rapidly as the scattering angle increases and becomes unaccessible to accurate measurement. This situation is illustrated in Fig. 6. Because of reasons given above, we deal with the trigonal reflections with ℓ odd only unless otherwise noted.

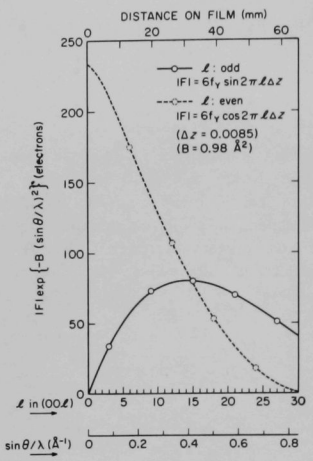

Fig. 6

General Characteristics of the Scattering-angle Dependence of the Intensities of the ℓ Even and ℓ Odd Reflections of Y_2C Are Shown Here Using the Structure Factors per Unit Cell for the (00ℓ) Reflections. The final parameter set was employed in the calculation. The ℓ even reflections are much stronger than the ℓ odd reflections at low scattering angles. In this region, the ℓ even reflections are inseparable from the cubic reflections. The intensities of ℓ even and ℓ odd become comparable near ℓ = 15, around which the ℓ even reflections tend to separate out from the cubic reflections. For ℓ > 15, the ℓ odd intensities become considerably stronger than the ℓ even intensities. The radial distance on the precession film is also given as a reference to the diffraction patterns shown in Figs. 3(a) through 5(b).

121-3330 Rev. 1

The topological analysis of the symmetry characteristics in the shift-vector distribution has played a most critical part in the structure analysis, as described in Ch. II. Here, one may surmise the difficulty we encountered by inspecting Figs. 3(a) through 5(b), which represent a transition from a simple case to a more complex case. In some other zones, the vector maps are by far more complex than the one shown in Fig. 5(b). These exceedingly complex cases are difficult to illustrate and are not shown.

As regards the shifting mode, it was immediately seen that the magnitude of the shift is larger, on the average, as the scattering angle increases. In the reciprocal planes containing the origin of the reciprocal lattice, both the direction and the magnitude of the shifting vector exhibit two twofold axial symmetries. However, no such symmetry exists in the intensity. These regularities were all we could find and provided no help in revealing the origin of the shifting.

A breakthrough came about when we found that the direction of the shift is parallel or antiparallel to the cubic body-diagonal axes or their projections onto the reciprocal zone of specific concern. This eventually revealed multidomain axial relations which could explain unambiguously all the observed shifts and intensities. This multidomain structure is described below.

As described in Ch. IV, our "single crystal" consists of one cubic single crystal and four trigonal single crystals. The axial interrelations among the cubic crystal and the trigonal crystals are illustrated in Fig. 7, where the [001] axes of four trigonal crystals are distinguished by means of subscripts: tri-I, tri-II, etc. The orientational correlations between

the cubic crystal and the trigonal crystal I are as follows: (a) the (111) plane of the cubic crystal lies parallel to the (001) or c-plane of the trigonal crystal; (b) the cubic $[1\bar{1}0]$ axis is parallel to the trigonal $[1\bar{1}0]$ axis. The criterion (a) defines the coherent interphase boundary between the cubic crystal and the trigonal crystal I (see Ch. VII.C). The c-axes of the trigonal crystals II, III, and IV are parallel to the $[\bar{1}11]$, $[1\bar{1}1]$, and $[11\bar{1}]$ axes of the cubic crystal, respectively.

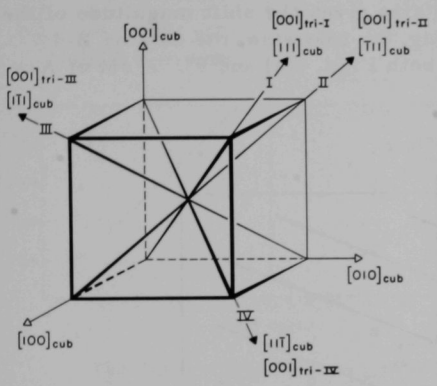

Fig. 7

Axial Relationships among the Trigonal Crystals Relative to the Cubic Crystal. The cubic axes have subscripts "cub." The trigonal c-axes of Type-I, -II, -III, and -IV domains are given with the subscripts tri-I, tri-II, tri-III, and tri-IV, respectively.

121-2685

We call the volume occupied by the trigonal crystal I the domain of Type I, and this nomenclature extends to other domains. The volumes of four domains are different from one another, causing a dismaying asymmetry of intensity in the precession photographs.

B. Precision Determination of Lattice Parameters

Small shifts of the trigonal reflections as shown in Figs. 3(b), 4(b), and 5(b) imply that the dimensions of the trigonal unit cell are approximately given by $a_{tri} \cong a_{cub}/\sqrt{2}$ and $c_{tri} \cong 2\sqrt{3}\, a_{cub}$, where the subscripts abbreviate trigonal and cubic. The precise determination of the trigonal lattice constants was not an easy task, since the trigonal reflections are generally very weak (see Ch. II.B).

The shift-vector maps Figs. 3(b), 4(b), and 5(b) show that the shifting directions are along the cubic principal axes. In some other zones, the vector directions have no simple relations with the principal axes. Nonetheless, a relatively straightforward deduction from the shift-vector analysis was that the a axis of the trigonal crystal should be very closely equal to the (110) spacing of the cubic crystal. The statistical numerical treatment to to a(trigonal) = 3.617 ± 0.002 Å, which turned out to be, within the accuracy cited above, equal to the d-spacing of the cubic (110) planes.

The c lattice constant of the trigonal phase was determined as follows. For instance, we select the shift-vector distribution of the Type-II domain as shown by the shaded arrows in Fig. 4(b). The shaded arrow

vectors are parallel or antiparallel to the cubic $[\bar{1}11]$ axis. The vectors labeled as A-1, A-2, A-3, etc., are pointing toward the cubic reflections $(1\bar{1}1)$, $(2\bar{2}2)$, $(3\bar{3}3)$, etc., respectively. The magnitudes of the shifts of A-1, A-2, and A-3 are plotted in Fig. 8. Because of a large uncertainty, the shift magnitude of the reflection A-4 is not given in Fig. 8. The trigonal indices of A-1, A-2, and A-3 are $(1\bar{1}\bar{5})$, $(2\bar{2}\bar{7})$, and $(3\bar{3}\bar{9})$, respectively. Therefore, in Fig. 8, the points representing the shift magnitudes of these three reflections should lie on a straight line. The intercepting point between this line and the trigonal $[00\bar{1}]$ axis gives the shift magnitude of the trigonal $(00\bar{3})$, Λ_1, as illustrated in Fig. 8. Likewise, the data on B-1 through B-6 led to the Λ_2 value [see both Figs. 4(b) and 8]. A set of Λ values was thus obtained.

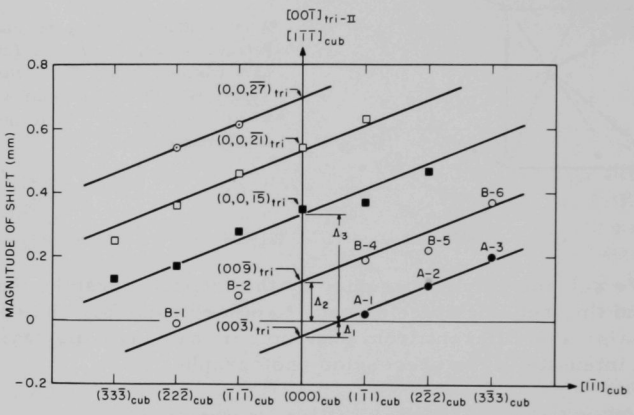

121-2684 Rev. 1

Fig. 8. Observed Magnitudes of the Shifts for the Domain-II Trigonal Reflections Which Appear in the Fig. 4(b) Zone Are Treated Here. The designations A-1, A-2, etc., are referred to the reflections with the same designations in Fig. 4(b). The statistically averaged shift values Λ_1, Λ_2, etc., are correlated in Fig. 9.

A least-squares treatment has been employed in obtaining the parameters of the straight lines of Fig. 8. As a corollary, for instance, the shift magnitude Λ_3 is more reliable than the data for $(0,0,\overline{15})$ alone. Now, these Λ values referring to respective ℓ's in (00ℓ) are shown in Fig. 9 which demonstrates excellent linear relationships in each Λ series. The ΔL value as given in Fig. 9 was obtained with a high accuracy because of the large number of observed data employed in the data deduction. The ΔL value has the following relation with $L(\bar{1}11)_{cub}$, representing the average distance on the film between the cubic reflections, (hk ℓ), and $(h\pm1, k\pm1, \ell\pm1)$: $L(\bar{1}11)_{cub} + \Delta L = L(006)_{tri}$, where $L(006)_{tri}$ is the distance between (hk ℓ) and (h, k, $\ell+6$) on the film. The observed results are

given in Fig. 9. The ratio between $L(\bar{1}11)_{cub}$ and $L(006)_{tri}$ is 1.0134 ± 0.0009, which gives the ratio between the interplanar spacing for the cubic $(\bar{1}11)$ planes and that for the trigonal (006) planes.

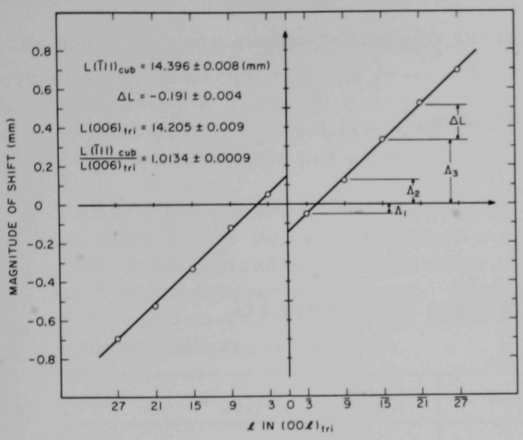

Fig. 9

Plots of the Λ Values in Fig. 8 against ℓ in the Trigonal Indices (00 ℓ). $L(\bar{1}11)_{cub}$ indicates an average distance between two nearest cubic diffraction spots along the $[\bar{1}11]_{cub}$ direction. $L(006)_{tri}$, which is equal to $L(\bar{1}11)_{cub} + \Delta L$, corresponds to the distance between two nearest trigonal spots along the $[\bar{1}11]_{cub}$ direction.

121-2690 Rev. 1

The interreflections distances on the precession photograph are influenced by a slight eccentricity in the crystal setting, variations in the film mount, differences in film shrinkages, etc. Hence, the data processing was carried out using the measured values obtained from the same film. Moreover, the ratio $L(\bar{1}11)_{cub}$ versus $L(006)_{tri}$ is, to a large extent, free from the experimental errors described above.

Based on this principle, the data processing was carried out with five reliable sets of data and the results are summarized in Table II, where unbelievably large numbers of measurements employed in the data deduction

TABLE II. Data Employed for Determining the Ratio between the Cubic (111) Spacing and the Trigonal (006) Spacing, Leading to a Highly Accurate c-lattice Constant of the Trigonal Structure. $L(111)_{cub}$ is the distance between the cubic (hkℓ) and (h ± 1, k ± 1, ℓ ± 1) reflections on the precession film. $L(006)_{tri}$ is the distance between the trigonal (hkℓ) and (h, k, ℓ ± 6) reflections and has a relation, $L(006)_{tri} = L(111)_{cub} + \Delta L$. Each group of data was acquired from the same film. Slight differences among $L(111)_{cub}$ are due to the variations in the experimental settings as explained in the text. The ratios, $L(111)_{cub}$ versus $L(006)_{tri}$, are highly reliable on account of eliminating most of the experimental variations. The standard deviations and the numbers of measurements employed are also given.

Domain	$L(111)_{cub}$ (mm)	ΔL (mm)	$L(006)_{tri}$ (mm)	$\frac{L(111)_{cub}}{L(006)_{tri}}$	Number of Data
II	14.396 ± 0.008	−0.191 ± 0.004	14.205 ± 0.009	1.0134 ± 0.0009	109
II	14.393 ± 0.009	−0.172 ± 0.002	14.221 ± 0.009	1.0121 ± 0.0009	113
III	14.425 ± 0.006	−0.204 ± 0.006	14.221 ± 0.009	1.0143 ± 0.0008	112
III	14.406 ± 0.007	−0.195 ± 0.004	14.211 ± 0.008	1.0137 ± 0.0007	117
IV	14.387 ± 0.008	−0.193 ± 0.005	14.194 ± 0.009	1.0136 ± 0.0008	64
			Weighted Average	1.0132 ± 0.0004	

should be noted. The final result that we have been after is the weighted average on the ratio values for $L(111)_{cub}$ versus $L(006)_{tri}$. It is 1.0132 ± 0.0004. Using the cubic lattice parameter obtained by means of the powder technique, one finally obtains the trigonal $\underline{c}$ spacing.

The lattice parameters of the trigonal structure are thus given as follows:

In the trigonal system, we have

$\underline{a}_{tri} = 3.617 \pm 0.002$ Å;

$\underline{c}_{tri} = 17.96 \pm 0.01$ Å;

$\underline{c}_{tri}/\underline{a}_{tri} = 4.965 \pm 0.003$.

In the rhombohedral system, the lattice parameters are

$\underline{a}_{rhomb} = 6.339 \pm 0.003$ Å;

$\underline{\alpha} = 33°09' \pm 4'$.

These results are of very high accuracy on account of the weak reflections with which the measurements were carried out. Our Y_2C values may be compared with the Ho_2C data, $\underline{a}_{rhomb} = 6.248 \pm 0.010$ Å and $\underline{\alpha} = 33°04' \pm 20'$ (Bacchella et al., 1966).

In Fig. 9, the intercepting value of the straight line with vertical axis is supposed to be zero, but it is -0.15 mm. This difference is very small but significant. It is partly explained by the absorption effect.

C. Determination of Space Group

A survey of the indices of the observed reflections failed to give any general extinction rule, except that the observed indices satisfy $-h+k+\ell = 3n$, implying the trigonal symmetry.

About 9,000 independent intensity measurements of the trigonal reflections with $\underline{\ell}$ odd were treated by the following crosslinking-weighted statistical averaging processes: an intrazone normalization on different time-exposured intensities; interzone intercorrelations; a data deduction using Friedel's law equivalency. The cubic reflections were frequently employed in the intensity standardization.

Since there are four trigonal single-crystal domains having different axial orientations, we obtained four sets of intensity values per reflection. The ratios among these four were taken, and the averages of these ratios were used to intercorrelate the intensity data of four domains.

The final intensity set was affirmative of the trigonal symmetry. We thus established the trigonal symmetry by all means. Since no general extinction was observed, the probable space group is D_3^7 - R32 (No. 155), C_{3v}^5 - R3m (No. 160), or D_{3d}^5 - $R\bar{3}m$ (No. 166) (International Tables, 1952).

The intensity data were then averaged out, utilizing the trigonal equivalency. Subsequently, the observed structure factors were obtained; these are listed in Table III, where 42 observed structure factors were deduced from approximately 9,000 intensity measurements (an average of about 200 measurements per structure factor!).

TABLE III. Observed and Calculated X-ray Structure Factors per Unit Cell of the ℓ Odd Reflections of the Trigonal Y_2C. The reflections marked with single asterisk were not included in the final least-squares refinement. Double asterisks designate unobserved reflections. Average standard deviation of the observed structure factors is about 5%.

Indices	F_{calc}	$\lvert F_{obs}\rvert$	Indices	F_{calc}	$\lvert F_{obs}\rvert$
003*	-49.8	**	0,0,21	67.2	72.5
101*	-1.6	<16.1	315	17.3	11.7
015	35.8	45.2	229	31.2	34.5
009*	65.4	**	137	-30.2	30.3
107	-65.5	69.5	0,2,19	-64.6	55.1
113*	-29.5	39.2	1,2,17	51.9	46.4
021*	1.3	<21.8	3,0,15	-53.0	58.7
0,1,11	-77.9	78.1	401*	0.8	<24.2
205	28.9	33.3	1,1,21	58.3	56.8
119	51.9	50.5	3,1,11	-40.0	41.7
027	-50.3	49.9	045*	14.7	<23.4
1,0,13	70.9	69.3	0,1,23	-64.5	61.6
0,0,15*	-85.3	102.7	407	-26.3	22.0
211*	1.4	<20.1	2,1,19	-56.0	52.6
2,0,11	-63.9	59.5	1,3,13	37.3	37.7
125	23.4	23.8	2,2,15	-45.9	44.5
217	-41.3	43.5	321*	0.6	<31.2
0,2,13	58.9	54.3	0,4,11	-34.8	30.4
303*	-19.5	<25.5	1,0,25	52.9	56.6
0,1,17	71.1	66.1	4,0,13	32.1	37.7
1,1,15	-72.1	70.9	413*	-11.0	<28.8
1,2,11	-54.0	54.5	3,1,17	39.3	42.0
309	36.5	35.8	3,0,21	43.8	51.5
1,0,19	-74.8	75.7	2,3,11	-30.3	29.3
2,1,13	50.1	48.8	419*	20.5	<27.9
223*	-16.6	<22.1	1,1,27	-46.8	51.1
2,0,17	60.4	59.7	0,1,29	40.5	48.3
131*	1.0	<26.8			

D. Statistical Structure Analysis

It should be reminded that we are dealing with the ℓ odd reflections only. Firstly, the intensities corrected for the Lorenz-polarization factors were arranged in order of increasing $\sin^2\theta$ and were grouped into appropriate equidivisional $\sin^2\theta$ regions in sequence. The intensity values within a given $\sin^2\theta$ region were averaged out. The resultant data are shown in Fig. 10. The procedure employed here is identical to the widely employed Wilson's zone-averaging method (Wilson, 1942).

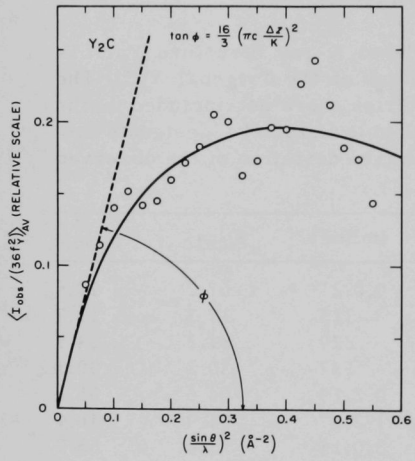

Fig. 10

A Graphical Representation of the Wilson-type, Zone-averaged Intensity Data. The solid line is a median curve for the averaged-out observed intensities whose values are given by small open circles. The $\Delta z/K$ value for Y in Y_2C was obtained from the tangential angle ϕ at $(\sin\theta/\lambda)^2 = 0$ using Eq. (22).

121-2693 Rev. 1

The solid-line curve in Fig. 10, a median of the observed points, starts from zero, increases very rapidly, and tends to fall off at high angles. This is in striking contrast with the usual Wilson plot, which is, in general, an inclined straight line starting from a nonzero value. The Wilson straight line is expected for a crystal structure consisting of a sufficiently large number of atoms at general positions. Our case is due, undoubtedly, to special arrangements of the atoms.

When small shifts in the positions of the reflections were neglected, the trigonal reflections with ℓ = 2n would lead to the face-centered cubic lattice of the yttrium atoms. However, the intensities of the trigonal reflections with ℓ = 2n fall off much faster with increasing $\sin\theta$ than does the cubic case (see Fig. 6). It appears that the trigonal reflections with ℓ odd build up their intensities at the expense of the ℓ = 2n intensities.

The predicament mentioned above implies that the yttrium atoms are slightly displaced from the face-centered cubic positions. Along this guide line, we interpret Fig. 10 as follows:

The trigonal unit cell should contain six Y atoms. The noncentrosymmetric space group R3m provides threefold positions for Y: (0, 0, 0; 1/3, 2/3, 2/3; 2/3, 1/3, 1/3) + (0, 0, $\underline{z}$). Two sets of the above coordinates are needed to accommodate two sets of three equivalent Y atoms. Hence, we have to determine two positional parameters, $\underline{z}_1$ and $\underline{z}_2$. In the centrosymmetric $R\bar{3}m$, we set $\underline{z}_1 = -\underline{z}_2$. This is also the case in the noncentrosymmetric R32. Hence, our Y-atom assignment in R32 is centrosymmetric. The choice of the origin in R3m is arbitrary. Hence, in R3m we may choose the origin so that $\underline{z}_1 = -\underline{z}_2$, which then becomes identical to the coordinate requirement in R32 and $R\bar{3}m$. In other words, insofar as the Y atoms are concerned, the choice among the three space groups is immaterial.

The structure factor in R3m excluding the carbon contribution is given by

$$F^2 = A^2 + B^2; \tag{13}$$

$$A = 3f_Y(\cos 2\pi\ell\underline{z}_1 + \cos 2\pi\ell\underline{z}_2); \tag{14}$$

$$B = 3f_Y(\sin 2\pi\ell\underline{z}_1 + \sin 2\pi\ell\underline{z}_2). \tag{15}$$

Equation (13) may be rewritten as

$$F^2 = 18f_Y^2\{1 + \cos 2\pi\ell(\underline{z}_1 - \underline{z}_2)\}. \tag{16}$$

Let us denote a small displacement from the special position as $\Delta\underline{z}$. From the cubic analogy, we set

$$\underline{z}_1 - \underline{z}_2 = 1/2 + 2\Delta\underline{z}, \tag{17}$$

which converts Eq. (16) into

$$|F|\ (\ell = \text{even}) = 6f_Y|\cos 2\pi\ell\Delta\underline{z}|, \tag{18}$$

and

$$|F|\ (\ell = \text{odd}) = 6f_Y|\sin 2\pi\ell\Delta\underline{z}|. \tag{19}$$

The last two equations delineate approximately the experimental result given in Fig. 10 and also the curves in Fig. 6.

Now, we again confine ourselves to the odd ℓ case, for which we use the relation

$$K^2I_{obs} = 36f_Y^2 \sin^2(2\pi\ell\Delta\underline{z}) \exp\left[-2B_Y\left(\frac{\sin\theta}{\lambda}\right)^2\right], \tag{20}$$

where K is the scale factor and I_{obs} is the observed intensity corrected for the Lorenz and polarization factors (by definition $I_{obs} = F^2_{obs}$). Based on Eq. (20), the averaging process employed for deriving the observed points in Fig. 10 corresponds to

$$K^2\left\langle I_{obs}/(36f_Y^2)\right\rangle_\ell = \left\langle \sin^2 2\pi\ell\Delta\underline{z}\right\rangle_\ell \exp\left\{-2B_Y\left(\frac{\sin\theta}{\lambda}\right)^2\right\}$$

$$= \frac{1}{2}\left(1 - \frac{\sin\chi}{\chi}\right)\exp\left\{-2B_Y\left(\frac{\sin\theta}{\lambda}\right)^2\right\}$$

$$= \frac{1}{2}\left(\frac{\chi^2}{3!} - \frac{\chi^4}{5!} + \ldots\right)\exp\left\{-2B_Y\left(\frac{\sin\theta}{\lambda}\right)^2\right\}, \qquad (21)$$

where

$$\chi = 8\pi\underline{c}(\Delta\underline{z})\frac{\sin\theta}{\lambda}$$

and $\underline{c}$ is the lattice constant. The solid curve in Fig. 10 follows roughly Eq. (21). For small θ, one approximates

$$\left\langle I_{obs}/(36f_Y^2)\right\rangle_\ell \cong \left(\frac{16}{3}\right)\left\{\frac{\pi\underline{c}(\Delta\underline{z})}{K}\right\}^2\left(\frac{\sin\theta}{\lambda}\right)^2 \qquad (22)$$

The tangent of the curve at $(\sin\theta/\lambda)^2 = 0$ in Fig. 10 is 1.60, with which $(\Delta\underline{z}/K)^2 = 0.96 \times 10^{-4}$ was obtained using Eq. (22).

A wavy nature of the observed points in Fig. 10 is explainable through the sin χ term in Eq. (21). However, owing to a relatively large experimental uncertainty, no reliable χ value could be deduced from the data in Fig. 10. Nonetheless, our interpretation here has now set up a good foundation for more refined structure analysis.

E. Statistical Refinement

Let us proceed with a simpler, yet better, statistical analysis than the Wilson-type approach. Firstly, we rewrite Eq. (20) in the form

$$I_{obs}/(36f_Y^2) = (1/K^2)\sin^2(2\pi\ell\Delta\underline{z})\exp\left\{-2B_Y\left(\frac{\sin\theta}{\lambda}\right)^2\right\}. \qquad (23)$$

Taking logarithms gives

$$\underline{\ell n}\left\{I_{obs}/(36f_Y^2)\right\} = \underline{\ell n}\left\{\frac{1}{K^2}\sin^2(2\pi\ell\Delta\underline{z})\right\} - 2B_Y\left(\frac{\sin\theta}{\lambda}\right)^2. \qquad (24)$$

We gather I_{obs}'s of the reflections with a given ℓ. The least-squares analysis of Eq. (24) gave the best values for $(1/K)|\sin(2\pi\ell\Delta\underline{z})|$ and B_Y. The absolute-value notation here will be dropped hereafter, since $\sin(2\pi\ell\Delta\underline{z})$ is always positive in the angular region of our concern. The procedure was applied to from $\ell = 3$ up to $\ell = 25$. A dozen B_Y values were thus obtained. A statistical average of those yielded $B_Y = 0.94$ Å^2.

When the $(1/K)\sin(2\pi\ell\Delta\underline{z})$ values are plotted as a function of ℓ, the resultant curve should be monotonically increasing at first, reach a maximum value, and then tend to fall off. The maximum point is attained when $2\pi\ell\Delta\underline{z} = \pi/2$, i.e., $\Delta\underline{z} = 1/(4\ell)$. At the same time, the maximum point gives $1/K$. Unfortunately, the observed data could barely reach the maximum value. Hence, a curve-fitting technique was employed to obtain K and $\Delta\underline{z}$.

This simple yet effective method is illustrated in Fig. 11, for which we write Eq. (23) as follows:

$$|F_{obs}| \Big/ \left[6 f_Y \exp\left\{ -B_Y \left(\frac{\sin\theta}{\lambda} \right)^2 \right\} \right] = \frac{1}{K} \sin(2\pi\ell\Delta\underline{z}). \qquad (25)$$

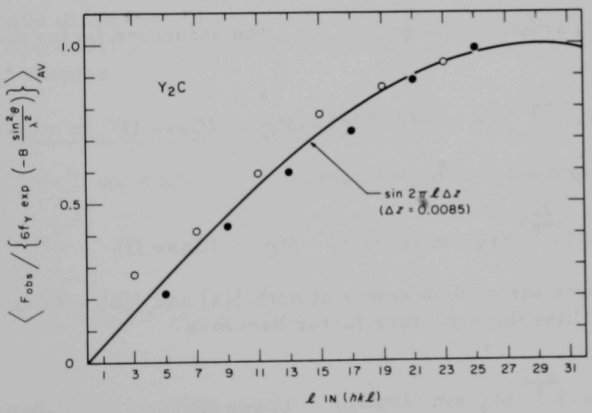

121-2691

Fig. 11. Determination of the Carbon Positional Parameter $\Delta\underline{z}$ Based on Eqs. (25) and (32). The scale factor K has been adjusted to unity. Open and shaded circles represent the observed points for $\ell = 4n - 1$ and $\ell = 4n + 1$, respectively. The solid line is a median curve for the observed points and is given by $(1/K)\sin(2\pi\ell\Delta\underline{z})$ with $K = 1$. Note that open circles are consistently above the solid curve, whereas shaded circles lie below the solid curve. These characteristics as well as the magnitudes of the deviations of the observed points from the solid curve were used to substantiate the validity of the Case I structure for Y_2C.

The maximum sine value takes place near $\ell = 29$. Therefore, $\Delta\underline{z} \cong 0.01$. The K value was about 1.0. Hence, $(\Delta\underline{z}/K)^2 \cong 1 \times 10^{-4}$, which is in agreement with the value obtained from the Wilson-type analysis.

F. Refinement of Structure

We have now obtained a good set of structure parameters for the yttrium atoms: $\Delta z = 0.01$, or $\underline{z} \equiv \underline{z}_1 = -\underline{z}_2 = 0.26$, and $B_Y = 0.94$ Å^2. Our task here is to refine these Y parameters and simultaneously to determine the parameters for the carbon atoms.

As regards the carbon assignment, we consider the following coordinate sets: both in R32 and R$\bar{3}$m, (0, 0, 0; 1/3, 2/3, 2/3; 2/3, 1/3, 1/3)+

3(a): 0, 0, 0

3(b): 0, 0, 1/2.

In R3m, we choose 3(a): 0, 0, $\underline{z}$, with $\underline{z} = 0$ or 1/2. Because of the special carbon positions under consideration, the choice of the space group becomes again immaterial.

If the carbon atoms occupy 3(a), the structure factor for ℓ odd is given by

$$F = (-1)^{\frac{\ell-1}{2}} 6f_Y \sin(2\pi\ell\Delta\underline{z}) - 3f_C \qquad \text{(Case I)}. \tag{26}$$

With the assignment to 3(b), we have

$$F = (-1)^{\frac{\ell-1}{2}} 6f_Y \sin(2\pi\ell\Delta\underline{z}) + 3f_C \qquad \text{(Case II)}. \tag{27}$$

When one places the carbon atoms at both 3(a) and 3(b) with an equal occupancy probability, the structure factor becomes

$$F = (-1)^{\frac{\ell-1}{2}} 6f_Y \sin(2\pi\ell\Delta\underline{z}) \qquad \text{(Case III)}. \tag{28}$$

The carbon contribution is revoked in the Case III. All cases stated above are computed for ℓ odd.

By means of Eqs. (26) to (28) and the least-squares method, the structural parameters were refined. The initial parameters employed were $\Delta\underline{z} = 0.01$ and $B_Y = B_C = 0.94$ Å^2. The discrepancy factors with these initial parameters were $R_1(0.086, 0.16, 0.10)$ and $R_2(0.009, 0.032, 0.014)$, respectively, for the Cases I, II, and III.

The Case I yielded the smallest discrepancy factors and is hence strongly favored. In Case I, one cycle of the least-squares refinement reduced $R_1 = 0.086$ to 0.056 and $R_2 = 0.009$ to 0.0055. For comparison, the one-cycle least-squares improvements in Case II were $R_1 = 0.16$ to 0.11 and $R_2 = 0.032$ to 0.016.

The second cycle in Case I gave $R_1 = 0.056$ and $R_2 = 0.0047$, both of which indicate no significant improvement. The final parameters in the Case I were

$$\Delta\underline{z} = 0.0085 \pm 0.0003,$$
$$\underline{z} = 0.2585 \pm 0.0003,$$
$$B_Y = 0.98 \pm 0.04 \text{ Å}^2,$$
$$B_C = 1.05 \pm 0.20 \text{ Å}^2,$$
$$K = 0.93 \pm 0.03.$$

The values reported for Ho_2C are $\underline{z} = 0.256 \pm 0.001$ and $B_Y = B_C = 0.32$ Å^2 (no accuracy is given) (Bacchella et al., 1966).

We have discarded Cases II and III on the basis of the R factor values. An additional strong endorsement for the Case I model is given in the following chapter.

G. Confirmation of Carbon Parameters

For Case I, we write

$$KF_{obs} = |F_{calc}|$$
$$= \left| (-1)^{\frac{\ell-1}{2}} 6f_Y \sin(2\pi\ell\Delta\underline{z}) \exp\left\{-B_Y\left(\frac{\sin\theta}{\lambda}\right)^2\right\} - 3f_C \exp\left\{-B_C\left(\frac{\sin\theta}{\lambda}\right)^2\right\} \right|. \quad (29)$$

The above equation is rearranged to

$$KF_{obs} \Big/ \left\{6f_Y \exp\left[-B_Y\left(\frac{\sin\theta}{\lambda}\right)^2\right]\right\}$$
$$= \left| (-1)^{\frac{\ell-1}{2}} \sin(2\pi\ell\Delta\underline{z}) - \frac{1}{2}\frac{f_C}{f_Y} \exp\left\{-(B_C - B_Y)\left(\frac{\sin\theta}{\lambda}\right)^2\right\} \right|$$
$$= \left| \sin(2\pi\underline{\ell}\Delta\underline{z}) + (-1)^{\frac{\ell+1}{2}} \frac{Z_C\hat{f}_C}{2Z_Y\hat{f}_Y} \exp\left\{-(B_C - B_Y)\left(\frac{\sin\theta}{\lambda}\right)^2\right\} \right|, \quad (30)$$

where $\hat{f}_C$ and $\hat{f}_Y$ are the unitary scattering factors and are given by $Z_C\hat{f}_C = f_C$ and $Z_Y\hat{f}_Y = f_Y$, where Z_C and Z_Y are the atomic numbers of C and Y, respectively.

Since $B_C \cong B_Y$, Eq. (30) simplifies to

$$KF_{obs}\Big/\left\{6f_Y \exp\left[-B_Y\left(\frac{\sin\theta}{\lambda}\right)^2\right]\right\} = \begin{cases} \sin(2\pi\ell\Delta\underline{z}) - \dfrac{1}{13}\dfrac{\hat{f}_C}{\hat{f}_Y} & (\ell = 4n+1), \\ \sin(2\pi\ell\Delta\underline{z}) + \dfrac{1}{13}\dfrac{\hat{f}_C}{\hat{f}_C} & (\ell = 4n-1). \end{cases} \tag{31}$$

The ratio $\hat{f}_C/\hat{f}_Y$ is relatively constant over our angular range. Let us then express as $\hat{f}_C/\hat{f}_Y = \alpha$. The right-hand side of Eq. (31) is hence dependent on $\ell\Delta\underline{z}$ only. We sum up all reflections with the same ℓ and divide the sum by the number of the reflections employed. This process is written as

$$\left\langle KF_{obs}\Big/\left\{6f_Y \exp\left[-B_Y\left(\frac{\sin\theta}{\lambda}\right)^2\right]\right\}\right\rangle_\ell = \begin{cases} \sin(2\pi\ell\Delta\underline{z}) - \dfrac{1}{13}\alpha & (\ell = 4n+1), \\ \sin(2\pi\ell\Delta\underline{z}) + \dfrac{1}{13}\alpha & (\ell = 4n-1). \end{cases} \tag{32}$$

This equation may be interpreted as Eq. (25) plus the carbon contribution. The experimental points in Fig. 11 are clearly in accordance with Eq. (32), namely, the experimental points for $\ell = 4n - 1$ lie consistently above the solid line representing Eq. (25) and those for $\ell = 4n + 1$ lie below the solid line. The observed magnitudes of these deviations gave approximately $\alpha = 1.8$, which is in good agreement with the calculated mean value, $\alpha = 1.76$, in the range from 0.25 to 0.75 in $(\sin\theta)/\lambda$.

If the Case II model were correct, the reversed signs should be assigned in the right-hand side of Eq. (32). The observed points for $\ell = 4n + 1$ in Fig. 11 would lie above the solid line and vice versa for $\ell = 4n - 1$. This is opposite to the observation. If the model for the Case III were correct, all observation points should lie right on the solid curve in Fig. 11. This is clearly not the case. We accordingly discard Cases II and III. The final atomic parameters are summarized in the Résumé Chapter.

VI. NEUTRON STUDY

The neutron diffraction pattern of yttrium hypocarbide obtained using an automatic multipurpose diffractometer (Atoji, 1964 and 1965) is shown in Fig. 12. The powdered sample employed here was prepared from the Lunex arc-melted buttons that had provided our single crystals used for the X-ray study. No coherent peaks due to the probable impurities (yttrium metal, graphite, Y_2C_3 and YC_2) were detectable in any of our neutron diffraction patterns.

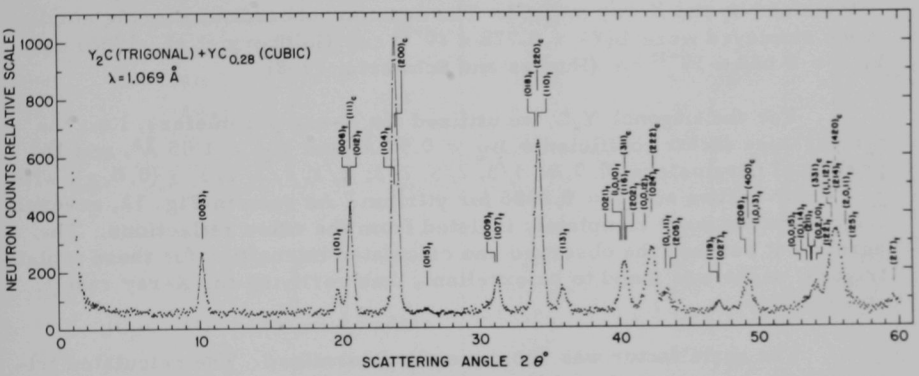

121-2805

Fig. 12. Neutron Powder Diffraction Pattern of a Mixed Phase of the Cubic $YC_{0.28}$ and the Trigonal Y_2C. Subscripts to the indices, "c" and "t," denote cubic and trigonal, respectively.

The powder sample was packed into a thin-walled cylindrical $Ti_{2.13}$ Zr holder which generates no coherent neutron scattering. The holder dimensions were 1 cm in diameter and 3.8 cm in the beam-bathed height. The packing density was 3.0 g/cm^3.

The total cross section obtained by means of the transmission cell (Atoji, 1964) was 11.3 ± 0.4 barns per YC_x at the neutron energy of 0.0716 eV or the neutron wavelength of 1.069 Å. The x value in YC_x was later determined as 0.43 from the coherent intensity analysis of our bulk neutron sample. At 0.0716 eV, the total cross section of Y is 8.0 barns (Goldberg et al., 1966) and that of C is 5.4 barns in various rare-earth carbides (Atoji, unpublished). Hence, the expected total cross section for $YC_{0.43}$ is 0.80 + 5.4 x 0.43 = 10.3, which is not significantly departed from the observed value 11.3 barns, particularly in view of a large uncertainty in the composition homogeneity.

The attenuation coefficient μ in $\exp(-\mu r)$ for our powder sample was 0.22 cm^{-1} x 0.5 cm = 0.11. Therefore, the angular dependence of the absorption factor could be neglected (International Tables, 1959).

The background of the diffraction pattern was satisfactorily accounted for by the sum of the elastic thermal diffuse scattering, the multiple scattering, and the instrumental scattering. Therefore, because of the absence of the paramagnetic scattering, yttrium hypocarbide should be very weakly paramagnetic or diamagnetic. The procedure of the background analysis has been fully described previously (Atoji, 1961 and 1967a).

The coherent peak intensities were analyzed utilizing the parameters determined by the X-ray method. The neutron coherent scattering amplitudes employed were $b(Y) = 0.778 \times 10^{-12}$ cm (Goldberg et al., 1966) and $b(C) = 0.662 \times 10^{-12}$ cm (Hughes and Schwartz, 1958).

For the trigonal Y_2C, we utilized the X-ray parameters, i.e., the temperature factor coefficients $B_Y = 0.98$ Å^2 and $B_C = 1.05$ Å^2, and the positional parameters $(0,0,0;\ 1/3, 2/3, 2/3;\ 2/3, 1/3, 1/3) \pm (0, 0, \underline{z})$, with $\underline{z} = 0$ for carbon and $\underline{z} = 0.2585$ for yttrium. As seen in Fig. 12, several trigonal peaks were completely isolated from the cubic reflections. The agreement between the observed and calculated intensities for those isolated trigonal peaks was found to be excellent, thus verifying the X-ray result conclusively.

The scale factor was subsequently determined. The calculated trigonal intensities were then subtracted from the observed peak intensities so as to obtain the cubic intensity values, for all cubic reflections are overlapped with the trigonal reflections. The resultant cubic intensities with all even in $(hk\ell)$ and those with all odd indices were treated separately, using the method similar to that described in Ch. IV. Two sets of these cubic intensities gave the same temperature factor, $B = 1.1 \pm 0.1$ Å^2, which is significantly smaller than the X-ray value of $B = 1.85 \pm 0.08$ Å^2. Also, the above data processing yielded the value $x = 0.28$ for YC_x with a high degree of reliability. It is not unreasonable to expect a smaller B value for smaller x, i.e., less carbon content.

With the parameters given above, all observed data were compared with the calculated values in Table IV. The final discrepancy factor value was

$$\frac{\sum |I_{obs} - I_{calc}|}{\sum I_{obs}} = 5.9\%,$$

which presents another confirmation of our X-ray structure. The other probable models discussed in Ch. IV.B gave significantly less satisfactory agreements.

TABLE IV. Observed and Calculated Neutron Diffraction Intensities for the Quenched Powder Sample of Yttrium Hypocarbide Which Is an Admixture of the Cubic $YC_{0.28}$ and the Trigonal Y_2C. The cubic reflections are designated by subscript c attached to their indices. The intensities are given in barns per unit cell. On the basis of this unit, within our experimental error, the scaling factor for the cubic $YC_{0.28}$ data is accidentally equal to the trigonal Y_2C scale factor.

Indices	I_{calc}		I_{obs}	Indices	I_{calc}		I_{obs}
003	930		900	0, 0, 15	113		
101	289		300	0, 1, 14	25		
006	181			211	68		
012	626	1474	1480	0, 2, 10	49		
$(111)_c$	667			122	164		
104	2818			$(331)_c$	257	3158	3690
$(200)_c$	960	3778	3780	1, 1, 12	709		
015	31		50	214	916		
009	0			$(420)_c$	625		
107	517	517	540	2, 0, 11	216		
018	1224			125	11		
110	1367	3501	3510	217	247		240
$(220)_c$	910			1, 0, 16	454		
113	417		430	128	335		
021	66			300	494		
1, 0, 10	93			$(422)_c$	498	1910	2110
116	264	1069	1070	0, 2, 13	9		
202	155			303	120		
$(311)_c$	491			0, 1, 17	23		
0, 0, 12	220			1, 1, 15	429		
024	841			0, 0, 18	8		
$(222)_c$	384	1847	2060	2, 0, 14	5		
0, 1, 11	392			2, 1, 10	32	807	770
205	10			306	91		
119	1			$(333)_c$	55		
027	211	212	200	$(511)_c$	164		
208	547			1, 2, 11	282		160
1, 0, 13	15	767	750				
$(400)_c$	205						

To recapitulate, our bulk neutron sample consisted of trigonal Y_2C and cubic $YC_{0.28}$. From the scale factors for these two structures, the average chemical formula for our bulk neutron sample was obtained as $YC_{0.43}$. The chemical analysis on the basis of random sampling of several arc-melted buttons gave, $YC_{0.39}$ (see Ch. III). The chemical composition of our polydomain single crystal is approximately given by $YC_{0.5}$. A considerable inhomogeneity of our arc-melted buttons should be noted.

VII. DISCUSSION

A. Layer Structures in YC_x

In Fig. 13, the crystal structure of the cubic YC_x is collated with the trigonal Y_2C structure. In this figure, A, B, and C represent the yttrium layers, whereas a, b, and c signify the carbon layers. The A, B, and C layer configurations are the same as the a, b, and c layers, respectively, except for the difference in occupants.

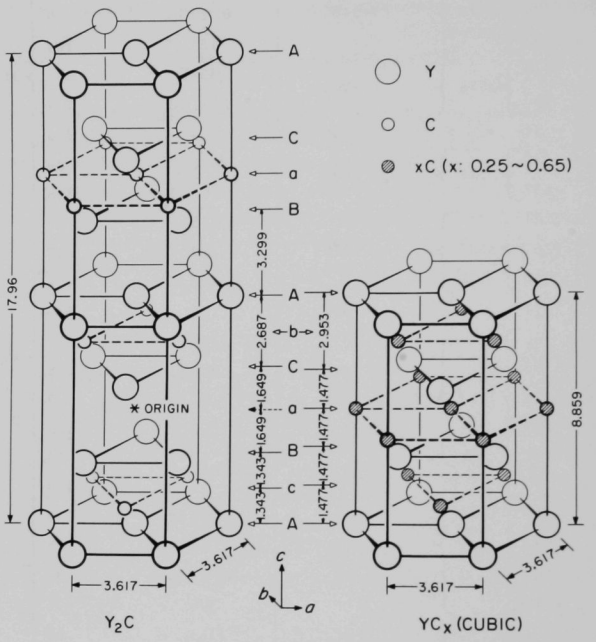

121-2682 Rev. 2

Fig. 13. Schematic Representations of the Cubic and Trigonal Structures of Yttrium Hypocarbide. The cubic structure is drawn on the trigonal coordinates. The capitals A, B, and C signify the yttrium layers, whereas the lower cases a, b, and c, designate the carbon layers. Pertinent interlayer distances are given.

In the cubic YC_x, the layer sequence along the [111] axis is $\{A\ \boxed{c}\ B\ \boxed{a}\ C\ \boxed{b}\ \ldots.\}$, where the $\{A\text{-}B\text{-}C\ldots.\}$ sequence delineates the cubic close-packing of the yttrium atoms and the $\{\boxed{c}\ \text{-}\ \boxed{a}\ \text{-}\ \boxed{b}\ \ldots.\}$ layers

designate the octahedral holes being partly occupied by the carbon atoms. Here, the interlayer distances are all equal to 1.477 Å, as shown in Fig. 13.

In the trigonal structure, the unit layer sequence may be written as $\{A\ c\ B\ \square\ C\ b\ A\ \square\ B\ a\ C\ \square \ldots.\}$. Here, $\square$ denotes the vacant layer, whereas a, b, and c designate the carbon layers with unit occupancy factor. Although the layer sequence in the trigonal Y_2C seems complex, it is almost identical to the cubic YC_x layer structure except for the following: every fourth layer (every other carbon layer) is completely vacant; the occupancy factor in the carbon layer is unity; the interlayer spacings are not all equal.

This last subject about the interlayer spacings is of particular interest. In the cubic-to-trigonal transformation, the spacing between the yttrium and carbon layers, or simply the hetero-interlayer distance, is smaller for the larger carbon population. The change in the occupancy parameter, from $x = 0.48$ to 1.00, varies the hetero-interlayer distance, from 1.477 to 1.343 Å, giving about 9.1% contraction. On the other hand, the occupancy parameter change, from $x = 0.48$ to zero, modulates the hetero-interlayer spacing from 1.477 Å to 1.649 Å, resulting in about 11.6% expansion. As a whole, the cubic-to-trigonal transformation expands the layer axial length (along [111] of cubic and [001] of trigonal) about 1.32%, while no change takes place in the intralayer interatomic distances. Subsequently, the volume of the crystal expands 1.32% in the cubic-to-trigonal transformation, i.e., a high-to-low temperature allotropic transition (see Ch. VIII). Hence, the crystal volume of the high-temperature disordered structure is smaller than the low-temperature ordered structure. The disposition here is indeed opposite to the commonly conceived structural conception.

In the cubic system, both Lallement (1966) and Spedding et al. (1958) have found that the cubic lattice spacing decreases as the carbon content increases. This is a striking contrast to the transition-metal carbide, where the reversed relation has been observed. Further discussion on this subject is given in Ch. VII.E.

B. Phase Transition

The phase diagram proposed by Lallement (1966) (see Fig. 14) suggests that the cubic hypocarbide is stable above about 1300-1400°C, below which the trigonal structure appears. The composition range of the cubic phase spans approximately the range $x = 0.35$-0.65 in YC_x, but a much narrower composition range is imposed upon the trigonal structure (meaning a very small leeway in the stoichiometry of Y_2C). Spedding et al. (1958) have found the existence of the cubic phase for $x \cong 0.25$-0.40. It is very likely that at certain temperatures the cubic phase could be stable in an extended range, $x \cong 0.25$-0.65, accommodating the findings of both Lallement (1966) and Spedding et al. (1958).

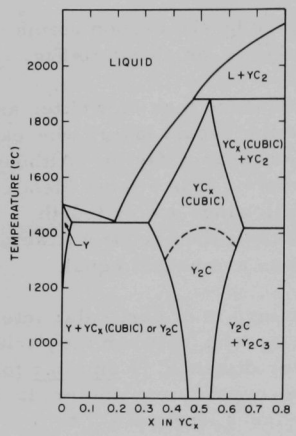

121-2694 Rev. 1

Fig. 14. Schematic Phase Diagram for the Yttrium-Carbon System (Lallement, 1966)

The transformation from cubic to trigonal may not be fully achieved in a fast cooling; hence, the cubic structure could exist in the quenched sample as a metastable phase. In our single crystal, the transformation has taken place partly. In other words, we have a restrained transient state, resulting in a two-phased or dimorphic single crystal.

In conjunction with the YC_x phase transition, recent work by Sarian and Criscione (1967) on the diffusion of carbon in $ZrC_{0.98}$ gives an estimate for just how mobile the carbon atoms would be in the metal matrix. From their diffusion data and lattice-constant values of ZrC at high temperatures (Elliott and Kempter, 1958), the average time that the carbon atom stays at a given lattice site in $ZrC_{0.98}$ is computed to be as short as 0.8×10^{-8} sec at 2200°C. It becomes exponentially longer as the temperature is lowered. Some typical values are 2.5×10^{-6} sec at 1700°C, 4.2×10^{-3} sec at 1300°C, 22 sec at 1000°C, and 2.2×10^{7} sec (nearly 2 yr) at 700°C. In deriving some of these values, the reported data have been extrapolated.

Another example we cite is that of body-centered cubic iron containing up to about 0.03 a/o carbon. The carbon atom stays at the interstitial site only for 1 sec, even at room temperature (Chalmers, 1959).

$ZrC_{0.98}$ provides a case where the vacant sites for carbon are exceedingly scarce. Iron containing a minute amount of carbon represents a case in which there exist highly abundant vacant interstices. The YC_x case may lie just about between these extremes. Hence, it is quite plausible that the mobility of carbon in the cubic Y matrix at high temperature is large enough to constitute a highly, disordered carbon distribution. On the other hand, the mobility of the carbon atoms is not fast enough to complete the cubic-trigonal transformation in a relatively rapid cooling.

Resnick and Seigle (1966) have given an interesting result for the diffusion of carbon in TaC. Azároff (1961a and 1961b) has discussed the diffusion process in the closest-packed crystals. The work of Rudy et al. (1967) on the phase transition of metal carbides comprehends the thermal analysis, the X-ray structure study, and metallographic observation.

C. Intercrystal Boundaries

Among probable transient boundaries between the cubic and trigonal crystals, the least interphase energy could be attainable by choosing the

cubic {111} and trigonal {001} planes as a common boundary interface, since the above planes are completely identical to each other in both the interatomic configuration and distance. The drawings given in Fig. 13 demonstrate this in a succinct manner. This cubic {111}-to-trigonal {001} boundary is a simple, yet typical, example of the coherent interphase interface, and is consistent with the intercrystal axial relations shown in Fig. 7.

The boundaries among four trigonal domains are not as straightforward as the cubic-trigonal boundary. Let us start from an ideal case. Suppose that the interatomic distances in the trigonal crystal are the same as those in the cubic crystal, except for the difference in the ordering scheme of the carbon atoms. Then, it is obvious that any atomic plane can be chosen as a coherent interface boundary between adjacent trigonal domains; that is to say, we have an arbitrary choice of the coherent isophase interfaces for the boundaries of four trigonal domains.

In the actual case, however, a small modulation in the interlayer distances takes place in the cubic-trigonal transformation. Hence, the coherent interface in the above idealized case becomes slightly incoherent. The energy associated with this incoherency should certainly be less than the stabilization energy in forming the trigonal crystals. The following example is of value in estimating the degree of incoherency in the isophase interfaces among the trigonal domains.

Although under certain conditions the generation of the trigonal domain may take place spontaneously at any region of the cubic crystal, for the sake of simplicity we assume that the trigonal crystals develop from the cubic {111} planes with an equal growth rate. In the aforementioned idealized case, in which no modulation takes place in the interlayer and intralayer interatomic distances, the coherent interfaces between the adjacent trigonal domains are the {108} planes (the {110} planes in the cubic description). However, because of a slight difference in the interlayer distance between the cubic and trigonal structures, the {108} planes of the adjacent trigonal domains split each other radially with the radial mutual splitting angle of 44'. This angle may be called a tilt angle, since in a conventional terminology the boundary of our concern may be said to be of a tilt boundary. Also, some call this a "subboundary" in a more general sense (Chalmers, 1959). The energy associated with such a small-angle tilt boundary would not be substantially large.

By the same token, in the generalized case, that is, when the growth rates of the trigonal domains are different from one another, the trigonal isophase interface is still a subboundary, and the degree of the incoherency should be as small as the equal domain-growth case.

In our multidomain single crystal it was found, through the diffraction intensity analysis, that the relative volumes of the cubic crystal and

those of the trigonal domains, I to IV, are 3.6, 0.40, 1.00, 0.48, and 0.91, respectively. Significant differences among four trigonal domain volumes suggest that the strain field and related factors could easily influence the growth rates of the trigonal domains in the cubic-to-trigonal transformation.

D. Bonding Configurations

The pertinent interatomic distances in the cubic and trigonal structures are listed in Table V. For obtaining a relative measure of bond strength, the bond numbers were computed using Pauling's (1960) semi-empirical equation

$$D(n) = D(1) - 0.60 \log_{10} n, \tag{33}$$

where D(1) is the single-bond distance and D(n) is the bond distance for the bond number n. Also, $D(n) = R_1(n) + R_2(n)$, where $R_1(n)$ and $R_2(n)$ are the bond radii of the atoms. We have chosen R(1) = 1.618 and 0.772 Å for Y and C, respectively. The R(1) value for Y was evaluated from the latest lattice constants of the Y metal (Gschneidner, 1961) and is slightly different from Pauling's value. The R(1) value for C was obtained from diamond. The resultant individual and total bond numbers are given in Table V.

TABLE V. Interatomic Distances and Corresponding Bond Numbers in the Cubic and Trigonal Yttrium Hypocarbides. The values for the YC_2 are also given. In the trigonal Y_2C, $Y\text{-}Y_I$ is the intralayer distance, $Y\text{-}Y_{II}$ is the interlayer distance across the carbon layer, and $Y\text{-}Y_{III}$ is the interlayer distance across the vacant layer.

Cubic YC_x (x = 0.48)	
C-6Y 2.558 Å (n = 0.525)	Y-6xC 2.558 Å (n = 0.525)
C-12xC 3.617 Å (n = 0)	Y-12Y 3.617 Å (n = 0.232)
$\sum$ n for C = 3.15	$\sum$ n for Y = 2.78 + 3.15x = 4.29
Trigonal Y_2C	
C-6Y 2.483 Å (n = 0.700)	Y-3C 2.483 Å (n = 0.700)
C-6C 3.617 Å (n = 0)	$Y\text{-}6Y_I$ 3.617 Å (n = 0.232)
$\sum$ n for C = 4.20	$Y\text{-}3Y_{II}$ 3.402 Å (n = 0.259)
	$Y\text{-}3Y_{III}$ 3.904 Å (n = 0.077)
	$\sum$ n for Y = 5.31
Tetragonal YC_2	
C-C 1.275 Å (n = 2.29)	Y-2C 2.447 Å (n = 0.804)
C-Y 2.447 Å (n = 0.804)	Y-8C 2.668 Å (n = 0.344)
C-4Y 2.668 Å (n = 0.344)	Y-4Y 3.664 Å (n = 0.194)
$\sum$ n for C = 4.47	$\sum$ n for Y = 5.14

The C-Y bond (n = 0.70) in Y_2C is substantially stronger than that in $YC_{0.48}$ (cubic) (n = 0.53). The Y-Y bond (n = 0.23) in $YC_{0.48}$ (cubic) remains the same in the intralayer distance $Y\text{-}Y_I$ in Y_2C. The interlayer Y-Y bond, between which carbon atoms intervene, $Y\text{-}Y_{II}$ (n = 0.26), is slightly stronger than the cubic Y-Y bond. On the other hand, the interlayer Y-Y bond across the vacant layer, $Y\text{-}Y_{III}$ (n = 0.08), is, however, largely weakened. In both the cubic and trigonal structures, the C-C bonds are all very weak.

The total bond numbers of C and Y in $YC_{0.48}$ (cubic) are 3.2 and 4.3, respectively, whereas they are 4.2 and 5.3 in Y_2C. Hence, in all accounts, the chemical bonding in Y_2C is substantially stronger than that in the cubic $YC_{0.48}$.

In the cubic structure, the statistical site symmetry of Y is m3m and that of C is also m3m. The octahedral symmetry is attained either in a time or space average sense. This statistically high symmetry breaks down to considerably lower symmetries in the trigonal structure.

In Y_2C, the site symmetry of C is centrosymmetric $\bar{3}$m and that of Y is noncentrosymmetric 3m. Hence, the bond configuration of C with respect to the surrounding Y atoms is that of slightly deformed octahedron. On the other hand, the bonding of Y in Y_2C is highly asymmetric (see Fig. 13). The Y-C bond configuration here is that of a trigonal pyramid with Y at its apex. The Y-Y bonds are also asymmetric, as may be seen from the wide differences among their bond numbers (see Table V).

The bond numbers in YC_2 (Atoji, 1961) are given in Table V for comparison. The total bond number of carbon in YC_2 is larger than that in Y_2C; the relation is reversed as regards the total bond number of Y. It appears that in comparison with Y_2C the bonding associated with C in YC_2 is enhanced at the expense of the bonding strength of Y. In fact, all carbon atoms in YC_2, a highly metallic compound, dimerize to form C_2 groups. Hence, the C-C intramolecular bond number of YC_2 (see Table V) was computed on the basis that it is a nonmetallic bond. There exists no such higher carbides in the transition-metal carbides. This implies that as regards the chemical-bonding aspect the carbon atoms in the rare-earth carbides play a much stronger role than those in the transition-metal carbides. This subject is again discussed in Ch. VIII.

So as to find the intercorrelation among the chemical-bond structures of YC_x, Y_2C, YC_2, and Y_2C_3 as appeared in the phase diagram (see Fig. 14), a literature survey of the crystal structure of Y_2C_3 was made. No report was found, although in some papers the rare-earth sesquicarbide structure was labeled as the Y_2C_3 type. More properly, it should have been stated that Y_2C_3 is probably isostructural to $(RE)_2C_3$ (Atoji and Williams, 1961).

Rundle (1948), utilizing Eq. (33) extensively, has given an illuminating interpretation on the bonding structures of the MX compounds (M = transition metal, and X = C, N, and O). The atomic-orbital treatment of the metallic bond by Altmann et al. (1957) together with Kimball's table for various bond hybrids (1940) render a fundamental account for the metallic-valency theory. Ern and Switendick (1965) and Lye and his co-workers (1965, 1966, and 1967) have extensively developed the band-structure analysis of the refractory MX compound. Keller's concept of the band structure (1960) may be applicable to the metal-carbide structure.

The crystal structure data for metal carbides and related compounds are becoming very numerous. Recent representative reviews, some of which include qualitative discussions on the chemical bond, are given by Senkin and Milliken (1963), Storms (1967), Williams (1966), Nowotony (1963), and Nowotony and Benesovsky (1967).

Many reliable data have recently become available on a long-disregarded subject, the physical properties of metal carbides. Some noted publications are as follows: The localized electron-density or ionic-state study by Nagakura et al. (1966) and of Hosoya et al. (1968); superconductivity (Sadagopan and Gatos, 1966); thermoionic work function (Wilson and McKee, 1967); scattering of electrons by vacancies in TiC_x (Williams, 1964); the X-ray emission spectra (Holliday, 1967); and the NMR study (Froidevaux and Rossier, 1967).

E. Related Structures

Firstly, we discuss some structural differences between the rare-earth hypocarbide and the transition-metal hypocarbide. We cite tantalum hypocarbide, Ta_2C, for the latter, since Ta_2C exhibits a phase transition similar to that of Y_2C and since the crystal structures of both phases of Ta_2C are known with good accuracy. So far, Ta_2C is the only case for which usable structural data of a transition metal hypocarbide exist.

The fundamental structure of Ta_2C is that of hexagonal close packing, whereas Y_2C has a cubic close-packed structure. Otherwise, the order-disorder transition of the carbon atoms in Ta_2C resembles that for the rare-earth hypocarbides. In the disordered structure of Ta_2C (Elliott, 1965), the tantalum atoms form a hexagonal close-packed lattice and the carbon atoms occupy randomly half of the octahedral interstices. The stacking structure of disordered Ta_2C may be represented by $\{A\ \boxed{c}\ B\ \boxed{c}\ A\ \boxed{c}\ B\ \ldots.\}$, where $\boxed{c}$ designates a half-filled carbon layer of the c-type configuration. In ordered Ta_2C (Bowman et al., 1965), the layer scheme is given by $\{A\ c\ B\ \square\ A\ c\ B\ \square\ A\ \ldots.\}$; here, $\square$ delineates an unoccupied layer as employed previously.

As seen in Table VI, in both Y_2C and Ho_2C, the disorder-to-order transition of the carbon atoms alters the metal-carbon bond number from 1/2 to 2/3, implying a considerable increase in the bond strength. On the other hand, in the ordered Ta_2C with the anti-CdI_2 type structure, the Ta-C bond number is 3/4, which is smaller than or equal to the Ta-C bond number in Ta_2C with the disordered carbon atoms.

TABLE VI. Metal-to-Carbon Bond Numbers in Some Representative Metal Hypocarbides. The single-bond radius R(1) of carbon is 0.772 Å. The probable bond number may be considered as a rounded-off value of the bond number.

Compound	Structure Type	Bond	Distance (Å)	R(1) for Metal (Å)	$\sum$ R(1) (Å)	Bond Number	Probable Bond Number
Y_2C[a]	Trigonal, anti-$CdCl_2$-type	Y-C	2.483	1.618	2.390	0.70	2/3
$YC_{0.48}$[a]	Cubic, NaCl-type	Y-C[f]	2.558	1.618	2.390	0.53	1/2
Ho_2C[b,c]	Trigonal, anti-$CdCl_2$-type	Ho-C	2.467	1.583	2.355	0.65	2/3
HoC_x,[c] $x \cong 0.30$	Cubic, NaCl-type	Ho-C[f]	2.495	1.583	2.355	0.59	1/2
~ 0.65			~2.475			~0.63	~2/3
Ta_2C[d]	Hexagonal, anti-CdI_2-type	Ta-C	2.186	1.343	2.115	0.76	3/4
Ta_2C[e]	Hexagonal, C disordered	Ta-C[f]	2.162	1.343	2.115	0.84	5/6
			~2.178			~0.79	~3/4

[a] This study.
[b] Bacchella et al. (1966).
[c] Lallement (1966).
[d] Bowman et al. (1965).
[e] As reviewed by Elliott (1965), there exists some discrepancies among the reported values. The range cited above covers the variations in the reported data.
[f] Distance between the metal and the octahedral interstitial site. Note that the octahedral sites are partially occupied by carbon atoms

In the ordered Ta_2C structure, the interlayer distance between two metal layers intervening the carbon layer is 2.505 Å, whereas the metal-metal interlayer distance across the vacant layer is 2.432 Å (Bowman et al., 1965). This relation is opposite to the Y_2C case.

In the Ta-C system, near the TaC composition, the cubic lattice increases in proportion to the carbon content (Bowman, 1961). In the cubic rare-earth hypocarbides, this relation is also reversed (Spedding et al., 1958; Lallement, 1966).

Therefore, in all cases described above, the carbon atom behaves as a typical interstitial atom in Ta_2C and lengthens the surrounding metal-metal distance. This is also the case in other transition-metal carbides. On the other hand, the carbon atom in the rare-earth hypocarbide strengthens the associating metal-metal bonding.

Now, we extend our review to the hypocarbides of other transition metals but still restrict ourselves to the Me_2C composition. A classification of these carbides is given in Table VII. The metals in the group IVA of the periodic table: Ti, Zr, and Hf, form NaCl-type carbides in the composition range from MeC to near Me_2C. The hypocarbides here do not have the ordered phase at room temperature. In the Cr-C system, the structures of Cr_3C_2, $Cr_{23}C_6$, Cr_7C_3, and Cr_3C_2 have been studied (Hansen, 1958; Elliott, 1965; Pearson, 1958; Pearson, 1967). However, the carbide with the structurally definable composition Cr_2C is not known.

TABLE VII. A Periodic-table Classification of the Ordered Structures of the Known Metal Hypocarbides with the Composition Me_2C and Having the High-temperature Carbon-disordered Phase. In all cases, the order-disorder transition affects slightly the structure of the metal matrix, which is approximated by either cubic close-packing (ccp) or by hexagonal close-packing (hcp). The ordered carbon distribution further classifies the structure types as follows: hcp-1, ζ-Fe_2N; hcp-2, ζ'-Fe_2N; hcp-3, ξ-Nb_2C; hcp-4, ϵ-Fe_2N; hcp-5, anti-CdI_2. The carbides of Ti, Zr, Hf, and Cr do not exhibit the structure types designated above.

IIIA	IVA	VA	VIA
Sc_2C	(Ti)	V_2C	(Cr)
ccp, anti-$CdCl_2$[a]		hcp-1[e,f]	
		hcp-2[g]	
		hcp-3[e]	
Y_2C	(Zr)	Nb_2C	Mo_2C
ccp, anti-$CdCl_2$[b,c]		hcp-2[g]	hcp-1[k,l]
		hcp-3[e]	
		hcp-4[e,h]	
	(Hf)	Ta_2C	W_2C
Ho_2C, Gd_2C		hcp-1[i]	hcp-1[l,m]
Dy_2C, Er_2C		hcp-5[j]	hcp-4[l]
ccp, anti-$CdCl_2$[c,d]			hcp-5[n]

[a] See Appendix.
[b] Present report (1968).
[c] Dean et al. (1964).
[d] Bacchella et al. (1966).
[e] Yvon et al. (1966).
[f] Yvon et al. (1967).
[g] Rudy and Brukl (1967).
[h] Terao (1964).
[i] Nagakura and Aihara (1967).
[j] Bowman et al. (1965).
[k] Parthé et al. (1963).
[l] Nagakura and Kikuchi (1966).
[m] Rudy and Windisch (1967).
[n] Butorina et al. (1960).

On the other hand, Sc, Y, rare earths, V, Nb, Ta, Mo, and W form Me_2C with a very small tolerance in the composition ratio. The crystal structures of these hypocarbides have been determined, but not with high accuracy except for the cases which we have cited in Table VI. The metal atoms Sc, Y, and rare earths form the cubic close-packed structure, and V, Nb, Ta, Mo, and W take part in the hexagonal close-packed matrix. Upon heating, an allotropic transition takes place due to the order-to-disorder change in the carbon positions. The transition may accompany a small distortion in the metal matrix, but does not alter the packing scheme of the metal atoms. Upon cooling the disordered compound, the carbon atoms settle down to certain positions, resulting in the various ordered structures listed in Table VII. When more than one ordered structure is given, all but one should be metastable at room temperature. The thermodynamic relation among these allotropic ordered structures has not been studied very thoroughly.

RÉSUMÉ OF STRUCTURE DATA

Chemical Formula	$YC_{0.28}$	$YC_{0.48}$	Y_2C*
Molecular Weight	92.28	94.69	189.9
Crystal Symmetry	Cubic	Cubic	Trigonal
Lattice Constants (Å)	a = 5.13 ± 0.01	$\underline{a}$ = 5.115 ± 0.002	$\underline{a}$ = 3.617 ± 0.002 $\underline{c}$ = 17.96 ± 0.01
Unit-cell Volume ($Å^3$)	135.0 ± 0.8	133.8 ± 0.1	203.4 ± 0.4
Chemical Formula Units per Unit Cell	4	4	3 (6 as $YC_{0.5}$)
Density (g/cm^3)	4.581	4.700	4.650
Space Group	O_h^5-Fm3m	O_h^5-Fm3m	D_{3d}^5-R$\bar{3}$m
Coordinates of Y	4(a)	4(a)	6(c), $\underline{z}$ = 0.2585 ± 0.0003
Coordinates of C	4(b)	4(b)	3(a)
Site Symmetry of Y	m3m	m3m	3m
Site Symmetry of C	m3m	m3m	$\bar{3}$m
Interatomic Distance Y-C (Å)	2.565 ± 0.005	2.558 ± 0.001	2.483 ± 0.003
Interatomic Distance Y-Y (Å)	3.627 ± 0.007	3.617 ± 0.002	3.402 ± 0.007 3.617 ± 0.002 3.904 ± 0.008
Temperature Factor Coefficient of Y ($Å^2$)	B = 1.1 ± 0.1	B = 1.85 ± 0.08	B = 0.98 ± 0.04
Temperature Factor Coefficient of C ($Å^2$)	B = 1.1 ± 0.1	B = 1.85 ± 0.08	B = 1.05 ± 0.20
Mean Debye Temperature** θ (°K)	230 ± 10	170 ± 5	233 ± 6

*In the rhombohedral coordinates, the lattice constants of Y_2C are a = 6.339 ± 0.003 Å and α = 33° 09' ±4'. This unit cell contains one Y_2C chemical unit. The coordinations of C and Y are 1(a) and 2(c) with $\underline{x}$ = 0.2585 ± 0.0003, respectively.

**For the derivation of the Debye temperature, see International Table (1959) and also Bernstein (1964).

APPENDIX

Crystal Structure of Sc_2C

Using the X-ray powder photographic method, Rassaerts et al. (1967) have determined the crystal structure of Sc_2C (their sample No. 60/40) as follows: a face-centered cubic structure with a = 9.44 Å for $Sc_{1.82}C$; space group, O_h^7-Fd3m (No. 227) (International Tables, 1952); the number of the Sc_2C units per unit cell = 16; Sc positions, 32(e), $(\underline{x}, \underline{x}, \underline{x})$ ○ with $\underline{x}$ = 3/8; carbon positions, 16(d), (5/8, 5/8, 5/8) ○ . The approximation, $Sc_{1.82}C$ = Sc_2C, is tolerable in the present discussion.

The observed scattering angles and the visually estimated intensities as reported by Rassaerts et al. (1967) are tabulated in Table VIII. Here, a universally accepted relative intensity designation (Peiser et al., 1955) prescribes approximately

vvs (or vs^+) for 100, vs for 90,

s for 80, ms (or m^+) for 70,

m for 60, wm (or m^- or w^+) for 50,

w for 40, vww (or w^-) for 30,

vw for 20, vvw (or vw^-) for 10.

TABLE VIII. Comparison between the Cubic and Trigonal Models for Sc_2C. Both the cubic and trigonal indices including those for the unobserved reflections are given. The dimensions of the trigonal unit cell were obtained from the cubic-cell dimension using the relations $\underline{a}_{tri} = \underline{a}_{cub}/2\sqrt{2}$ and $\underline{c}_{tri} = \sqrt{3}\,\underline{a}_{cub}$. Values of $2\theta_{obs}$ based on the data of Rassaerts et al. (1967) are listed, so that one can estimate the degree of overlapping among proximate reflections. Observed intensities, I_{obs}, are those given by Rassaerts et al. (1967). The calculated intensities per chemical formula unit, Sc_2C, were computed using the following parameters: a thermal parameter B = 1.0 $Å^2$ for all cases; a coordinate parameter for Sc in the trigonal model, $\underline{z}$ = 0.26.

Indices		$2\theta_{obs}$	$2\theta_{calc}$		$I_{calc} \times 10^{-2}$	
Cubic	Trigonal	(°)	(°)	I_{obs}	Cubic	Trigonal
111	003	16.2	16.3	w	51	277
311	101	-	31.4	*	18	4
222	012 006	32.9	32.9	vs+	1197	882 253 } 1135
400	104	38.2	38.1	vs	904	854
331	015	-	41.7	*	6	22
333 511	107 009	50.3	50.2	vw	1 3 } 4	80 18 } 98

TABLE VIII. (Contd.)

Indices		$2\theta_{obs}$ (°)	$2\theta_{calc}$ (°)	I_{obs}	$I_{calc} \times 10^{-2}$	
Cubic	Trigonal				Cubic	Trigonal
440	110, 018	55.0	55.0	s	556	248, 196 } 444
531	113	-	57.8	*	3	29
533	021	-	64.8	*	1	0
622	202, 116, 1, 0, 10	65.6	65.6	ms	347	85, 148, 54 } 287
444	024, 0, 0, 12	69.0	68.9	mw	141	100, 20 } 120
551, 711	205, 0, 1, 11	71.4	71.4	vvw	1, 1 } 2	4, 42 } 46
553, 731	027, 119	77.6	77.7	vvw	1, 1 } 2	15, 22 } 37
800	208	81.5	81.6	w-	58	46
733	1, 0, 13	-	83.9	*	0	18
555, 751	211, 0, 0, 15	-	90.0	*	0, 1 } 1	0, 10 } 10
622	122, 0, 2, 10, 0, 1, 14	90.7	90.8	mw	116	57, 18, 10 } 85
840	214, 1, 1, 12	93.8	93.8	m	159	75, 45 } 120
753, 911	125, 2, 0, 11	96.0	96.2	vvw	1, 0 } 1	3, 17 } 20
931	217	-	102.4	*	1	16
844	300, 128, 1, 0, 16	106.2	106.3	m-	132	33, 52, 11 } 96
755, 771, 933	303, 0, 2, 13	108.6	108.7	vvw	0, 0, 0 } 1	4, 11 } 15
773, 951	1, 1, 15, 0, 1, 17	115.2	115.3	vw	0, 1 } 1	43, 16 } 59
666, 10, 2, 2	306, 2, 1, 10, 2, 0, 14, 0, 0, 18	116.0	116.1	mw	29, 86 } 115	1, 36, 27, 8 } 72
953	1, 2, 11	122.1	122.2	vvw	1	29
775, 11, 1, 1	309	130.1	129.9	vvw	0, 0 } 1	11
880	220, 0, 2, 16	134.8	134.9	w	75	38, 13 } 51

TABLE VIII. (Contd.)

Indices		$2\theta_{obs}$ (°)	$2\theta_{calc}$ (°)	I_{obs}	$I_{calc} \times 10^{-2}$	
Cubic	Trigonal				Cubic	Trigonal
955	223				0	5
971	2, 1, 13	138.1	138.4	w-	1 (2)	26 (66)
11, 3, 1	1, 0, 19				1	35
973	131				1	0
11, 3, 3	2, 0, 17	-	148.6	*	0 (1)	26 (26)
	312					69
	226					60
10, 6, 2	1, 2, 14	150.1	150.0	ms	281	25 (163)
	1, 1, 18					9
	134					128
884	3, 0, 12	156.9	156.9	s-	270 (337)	77 (214)
12, 0, 0	0, 1, 20				67	9

*The intensities for those reflections are not given by Rasserts et al., probably because they are too weak to be observable or overlapped with the adjacent strong reflections.

As regards the cubic indices in Table VIII, Table 3 of that paper of Rassaerts et al. has omitted a number of all-odd reflections such as (311), (331), (531), (533), (733), (555), (751), etc. In Table VIII the data have been compiled for all cubic reflections specified by the given space group. The cubic intensitites were computed based on the model of Rassaerts et al. The Debye-Waller temperature-factor coefficient, $B = 1.0$ Å^2, was assumed here by analogy with that for Y_2C. For our purpose, this assignment of temperature parameter is rather immaterial.

Firstly, the calculated cubic intensities suggest that most of the observed all-odd reflections are actually too weak to be observable. For instance, I_{calc} of the doublet (333) and (511) is less than 1% of I_{calc} of the nearby strong reflection (440), whereas the observed intensity ratio should be around 25% for this value. There are many other cases similar to the above example, as is seen in Table VIII.

If the intensity designation of Rassaerts et al. is vastly different from the conventional one, then quite a few unobserved all-odd reflections should have been observed. For instance, since the doublet (333) and (511), with $\Sigma I_{calc} = 4$, has been observed, the reflection (331) with $I_{calc} = 6$ should have also been observed and could be well resolved from the neighboring reflections. It appears that the cubic model is not at all well justified.

It is an outright speculation that the trigonal Y_2C-type structure may provide a better interpretation than the cubic model. The trigonal structure of Sc_2C was constructed using the lattice conversions $a_{tri} = a_{cub}/2\sqrt{2}$ and $c_{tri} = \sqrt{3}\, a_{cub}$. As seen in the case of holmium and yttrium hypocarbides, this approximation is quite permissible for our comparative purpose. By the same token, we assume the z parameter of 0.26 for Sc and B = 1.0 Å^2 for both Sc and C.

The resultant calculated intensities clearly demonstrate by far a better agreement with the observed data than the cubic case. It is therefore highly probable that Sc_2C (No. 60/40 sample of Rassaerts et al.) is isostructural to the trigonal Y_2C. It should be noted that some Sc_xC (x = 2-3) samples of Rassaerts et al., such as $Sc_{2.4}C$ (No. 80/20 in their sample designation) appears to be isostructural to the cubic YC_x.

ACKNOWLEDGMENTS

The authors are grateful to Mr. D. Tresidder who carried out most of the diffraction intensity measurements, a majority of the film distance measurements, and a part of the data processing. One of the authors (M. A.) wishes to express his sincere thanks to the following collaborators and colleagues: Drs. F. H. Spedding, A. H. Daane, and K. Gschneidner, Jr., supplied the yttrium hypocarbide sample used in the earlier stage of the study. Dr. J. L. Moriaty prepared the sample used for the major part of the study. The preliminary neutron diffraction experiment was carried out at the Oak Ridge National Laboratory through the courtesy of Dr. H. A. Levy. Dr. S. S. Sidhu (deceased) was helpful in arranging the earlier neutron experiment at Argonne. Dr. Yves Jeannin pursued some trial X-ray work that led to the single crystal study. Mr. J. Gvildys was instrumental in the computer data processing. Drs. H. G. Norment, J. Karle, and Deane K. Smith provided their computer programs. Dr. C. P. Kempter informed us of the French progress on the subject, Messrs. E. E. Klocek, S. M. Johnson, W. T. Willis, Jr., J. E. Slattery, D. G. Wozniak, and A. Jackowski have been untiringly associated with various phases of the neutron and X-ray instrumentational work. The analytical and spectroscopic groups of the ANL Chemistry Division analyzed carefully a number of the YC_x samples.

REFERENCES

Altmann, S. L. Coulson, C. A., and Hume-Rothery, W., *On the Relation between Bond Hybrids and the Metallic Structures*, Proc. Roy. Soc. (London) *A240*, 145 (1957).

Atoji, M., *Neutron Diffraction Studies of CaC_2, YC_2, LaC_2, CeC_2, TbC_2, YbC_2, LuC_2, and UC_2*, J. Chem. Phys. *35*, 1950 (1961).

Atoji, M., and Williams, D. E., *Neutron-diffraction Studies of La_2C_3, Ce_2C_3, Pr_2C_3, and Tb_2C_3*, J. Chem. Phys. *35*, 1960 (1961).

Atoji, M., *Some New Structure Data on the Metal Carbides*, American Crystallographic Association, Annual Meeting (June 18-22), Villanova, Pennsylvania (1962a).

Atoji, M., *Neutron Diffraction Studies of Higher Carbides of Heavy Metals*, J. Phys. Soc. Japan *17*, Suppl. B-II, 395 (1962b).

Atoji, M., *A Multipurpose Neutron Diffractometer*, ANL-6920 (1964).

Atoji, M., *Multipurpose Neutron-diffraction Instrumentations*, Nucl. Instr. Methods *35*, 13 (1965).

Atoji, M., *Crystal and Magnetic Structures of CeC_2, PrC_2, and NdC_2*, Phys. Rev. Letters *22*, 21 (1966a).

Atoji, M., *Magnetic Structures of TbC_2 and HoC_2*, Phys. Rev. Letters *23*, 208 (1966b).

Atoji, M., and Gvildys, J., *Modulated Reciprocal Crystal-lattice and Diffractometric Computer Program*, ANL-7147 (1966).

Atoji, M., *Magnetic and Crystal Structures of CeC_2, PrC_2, NdC_2, TbC_2, and HoC_2 at Low Temperatures*, J. Chem. Phys. *46*, 1891 (1967a).

Atoji, M., *Neutron Diffraction Study of Ce_2C_3 at Low Temperatures*, J. Chem. Phys. *46*, 4148 (1967b).

Atoji, M., *Neutron Diffraction Study of UC_2 at 300-5°K*, J. Chem. Phys. *47*, 1188 (1967c).

Atoji, M., *The Magnetic Structure of DyC_2*, J. Chem. Phys., in press (1968).

Azároff, L. V., *Role of Crystal Structure in Diffisuion. I. Diffusion Paths in Closest-packed Crystals*, J. Appl. Phys. *32*, 1658 (1961a).

Azároff, L. V., *Role of Crystal Structure in Diffusion. II. Activation Energies for Diffusion in Closest-packed Structures*, J. Appl. Phys. *32*, 1663 (1961b).

Bacchella, G. L., Mériel, P., Pinot, M., and Lallement, R., *Étude par Diffraction de Neutrons de Ho_2C*, Bull. Soc. Franç. Minér. Crist. *89*, 226 (1966).

Bernstein, H., *Debye Temperatures and Thermal Properties of HfB_2, ZrB_2, HfC, and ZrC from X-ray Diffraction Measurements*, Nuclear Metallurgy *10*, 609 (1964).

Bowman, A. L., *The Variation of Lattice Parameter with Carbon Content of Tantalum Carbide*, J. Phys. Chem. *65*, 1596 (1961).

Bowman, A. L., Wallace, T. C., Yarnell, J. L., Wenzel, R. G., and Storms, E. K., *The Crystal Structures of V_2C and Ta_2C*, Acta Cryst. *19*, 6 (1965).

Burbank, R. D., and Knox, K., *Lorenz Polarization Absorption Corrections in the X-ray Precession Method*, Rev. Sci. Instr. *33*, 218 (1962).

Butorina, L. N., and Pinsker, Z. G., *Electron-Diffraction Study of W_2C*, Soviet Phys. Cryst. *5*, 560 (1960).

Chalmers, B., *Physical Metallurgy*, pp. 110-138, John Wiley and Sons, New York (1959).

Cromer, D. T., Larson, A. C., and Waber, J. T., *Hartree Scattering Factors for Elements 2 through 98 and for Several Ions*, LA-2987 (1963).

Dean, G., Lallement, R., Lorenzelli, R., and Pascard, R., *Existence et Structure d'une Phase M_2C dans les Systèmes Terres Rares Yttriques-Carbone*, Compt. rend. *259*, 2442 (1964).

Elliott, R. O., and Kempter, C. P., *Thermal Expansion of Some Transition Metal Carbides*, J. Phys. Chem. *62*, 630 (1958).

Elliott, R. P., *Constitution of Binary Alloys, First Supplement*, McGraw-Hill, New York (1965).

Ern, V., and Switendick, A. C., *Electronic Band Structure of TiC, TiN, and TiO*, Phys. Rev. *137*, A1927 (1965).

Frazer, J. W., and Holzmann, R. T., *Micro Determination of Carbon in Metals*, UCRL-6020 (1960).

Froidevaux, C., and Rossier, D., *N.M.R. Investigation of the Atomic and Electronic Structure of Vanadium and Niobium Carbides*, J. Phys. Chem. Solids *28*, 1197 (1967).

Goldberg, M. D., Mughabghab, S. F., Magurno, B. A., and May, V. M., *Neutron Cross Sections, Vol. IIA, Z = 21 to 40*, BNL-325, 2nd ed., Suppl. No. 2 (1966).

Gschneidner, K. A., Jr., *Rare Earth Alloys*, D. Van Nostrand Co., Princeton (1961).

Hansen, M., *Constitution of Binary Alloys*, 2nd ed., McGraw-Hill, New York (1958).

Holliday, J. E., *Investigation of the Carbon K and Metal Emission Bands and Bonding for Stoichiometric and Nonstoichiometric Carbides*, J. Appl. Phys. *38*, 4720 (1967).

Hosoya, S., Yamagishi, T., and Tokonami, M., *Study of Electron State in Vanadium Nitride by Intensity Measurements of X-ray Diffraction*, J. Phys. Soc. Japan *24*, 363 (1968).

Hughes, D. J., and Schwartz, R. B., *Neutron Cross Sections*, BNL-325, 2nd ed. (1958).

International Tables for X-ray Crystallography, Kynoch Press, Birmingham, England, Vol. I. (1952).

International Tables for X-ray Crystallography, Kynoch Press, Birmingham, England, Vol. II. (1959).

International Tables for X-ray Crystallography, Kynoch Press, Birmingham, England, Vol. III. (1962).

Keller, J. M., *Conduction Electrons in Sodium Tungsten Bronze*, J. Chem. Phys. *33*, 232 (1960).

Kimball, G. E., *Directed Valence*, J. Chem. Phys. *8*, 188 (1940).

Kikuchi, M., *The Crystal Structures of Transition Metal Carbides*, Thesis, Tokyo Institute of Technology (1966).

Lallement, R., *Existence et Structure des Monocarbures de Terres Rares; Étude de Leurs Propriétés Magnétiques a Basses Températures*, Centre d'Études Nucléaires de Fontenay-Aux-Roses Rapport, CEA-R 3043 (1966).

Lye, R. G., *The Thermoelectric Power of Titanium Carbide*, J. Phys. Chem. Solids *26*, 407 (1965).

Lye, R. G., and Logothetis, E. M., *Optical Properties and Band Structure of Titanium Carbide*, Phys. Rev. *147*, 622 (1966).

Lye, R. G. (in Gilman, J. J., and Tiller, W. A., ed. "Atomic and Electronic Structure of Metals"), *Band Structure and Bonding in Titanium Carbide*, American Society of Metals, Ohio (1967).

Nagakura, S., *The Crystal Structures of Transition Metal Carbides and Nitrides*, Zairyokagaku *3*, 70 (1966) (in Japanese).

Nagakura, S., and Aihara, I., private communication (1967).

Nagakura, S., Kikuchi, M., and Oketani, S., *Electron Diffraction Determination of the Ionization of the Carbon Atom in β-Mo_2C Crystal*, Acta Cryst. *21*, 1009 (1966).

Norment, H. G., *An X-ray Diffraction Data Reduction Program for the IBM 704 and 7090*, NRL-5739 (1962).

Nowotny, H. (in Beck, P. A., ed., "Electronic Structure and Alloy Chemistry of the Transition Elements"), *Alloy Chemistry of Transition Element Borides, Carbides, Nitrides, Aluminides, and Silicides*, Interscience Publishers, New York (1963).

Nowotny, H., and Benesovsky, F. (in Rudman, P. S., Stringer, J., and Jaffee, R. I., ed., "Phase Stability in Metals and Alloys"), *Phase Stability and Crystal Chemistry of Complex Compounds Containing Transition Elements and Nonmetals*, McGraw-Hill, New York (1967).

Parthé, E., and Sadagopan, V., *The Structure of Dimolybdenum Carbide by Neutron Diffraction Technique*, Acta Cryst. *16*, 202 (1963).

Pauling, L., *The Nature of the Chemical Bond*, 3rd ed., Cornell University Press, New York (1960).

Pearson, W. B., *A Handbook of Lattice Spacings and Structures of Metals and Alloys*, Pergamon, Oxford, Vol. I (1958); Vol. II (1967).

Peiser, H. S., Rooksby, H. P., and Wilson, A. J. C., *X-ray Diffraction by Polycrystalline Materials*, The Institute of Physics, London (1955).

Rassaerts, H., Nowotny, H., Vinek, G., and Benesovsky, F., *Zum System Scandium-Kohlenstoff, 1.Mitt.*, Monatsh. Chem. *98*, 460 (1967).

Resnick, R., and Seigle, L., *The Diffusion of Carbon in Tantalum Monocarbide*, Trans. Met. Soc. AIME *236*, 1732 (1966).

Rudy, E., and Brukl, C. E., *Lower-temperature Modifications of Nb_2C and V_2C*, J. Amer. Cer. Soc. *50*, 265 (1967).

Rudy, E., and Windisch, St., *Evidence for Zeta Fe_2N-type Sublattice Order in W_2C at Intermediate Temperatures*, J. Amer. Cer. Soc. *50*, 272 (1967).

Rudy, E., Windisch, St., Stosick, A. J., and Hoffman, J. R., *The Constitution of Binary Molybdenum-Carbon Alloys*, Trans. Met. Soc. AIME *239*, 1247 (1967).

Rundle, R. E., *A New Interpretation of Interstitial Compounds - Metallic Carbides, Nitrides and Oxides of Composition MX*, Acta Cryst. *1*, 180 (1948).

Sadagopan, V., and Gatos, H. C., *Superconductivity in the Transition Metal Carbides: $Mo_{4.8}Si_3C_{0.6}$, $Mo_{0.95}Hf_{0.05}C_{0.75}$ and Mo_2C*, J. Phys. Chem. Solids *27*, 235 (1966).

Sarian, S., and Criscione, J. M., *Diffusion of Carbon through Zirconium Monocarbide*, J. Appl. Phys. *38*, 1794 (1967).

Senkin, J. E., and Milliken, M. T., *Some Physical, Mechanical, and Thermodynamic Properties of Transition Metal Refractory Carbides: A Bibliography*, UCRL-7284 (1963).

Spedding, F. H., Gschneidner, K., Jr., and Daane, A. H., *The Crystal Structures of Some of the Rare Earth Carbides*, J. Am. Chem. Soc. *80*, 4499 (1958).

Storms, E. K., *The Refractory Carbides*, Academic Press, New York (1967).

Terao, N., *Structure des Carbures de Niobium*, Japan, J. Appl. Phys. *3*, 104 (1964).

Williams, W. S., *Scattering of Electrons by Vacancies in Nonstoichiometric Crystals of Titanium Carbide*, Phys. Rev. *135A*, 505 (1964).

Williams, W. S., *Cubic Carbides*, Science *152*, 34 (1966).

Wilson, A. J. C., *Determination of Absolute from Relative X-ray Intensity Data*, Nature *150*, 152 (1942).

Wilson, R. G., and McKee, W. E., *Vacuum Thermionic Work Functions and Thermal Stability of TaB_2, ZrC, Mo_2C, $MoSi_2$, $TaSi_2$, and WSi_2*, J. Appl. Phys. *38*, 1716 (1967).

Yvon, K., Rieger, W., and Nowotny, H., *Die Kristallstruktur von V_2C*, Monatsh. Chem. *97*, 689 (1966).

Yvon, K., Nowotny, H., and Kieffer, R., *Die Kristallstruktur der Subcarbide von Übergangsmetallen*, Monatsch. Chem. *98*, 34 (1967).

NOTE ADDED IN PROOF: CORRECTION FOR ANOMALOUS DISPERSION

A. Introduction

The wavelength of the MoKα radiation (0.7107 Å) employed for the present single-crystal work lies in the proximity of the K absorption-edge wavelength of Y (at 0.7276 Å). This would result in a large correction for anomalous dispersion to the scattering factor of Y, namely, f_Y. In fact, the dispersion values are very large, that is,

$$\Delta f'_Y = -2.96 \text{ and } \Delta f''_Y = 4.00 \text{ in } f_Y + \Delta f'_Y + i\Delta f''_Y$$

(Cromer, 1965). The $\Delta f'_Y$ and $\Delta f''_Y$ values do not vary significantly in the scattering angular range of our concern. The dispersion correction for f_C should be negligibly small. It is known that the dispersion correction may modulate appreciably the scale and temperature factors, but not atomic position parameters in centric crystals (Templeton, 1955).

However, the dispersion correction for f_Y in our case is considerably larger than f_C in most of our scattering angular range (see Table I). Also, $\Delta f'_Y$ amounts to as much as 10 to 20% of f_Y (see also Table I). Such a large dispersion correction might modulate significantly not only the scale and temperature factors, but also the atomic parameters. Hence, a complete structure analysis of the cubic and trigonal yttrium hypocarbide has been carried out using the dispersion-corrected scattering factors. In spite of the large dispersion correction, the results indicated no significant changes in the atomic coordinates and relatively small changes in the scale and temperature factors. The details are described in the following. The dispersion-corrected equations labeled as (1'), (2'), etc., correspond respectively to the nondispersion equations, Eqs. (1), (2), etc. The same notation has been applied to the tables and the figures.

B. Cubic YC_x Structure with Dispersion Correction

With the dispersion terms, the NaCl-type structure factor per unit cell for YC_x (cubic) is written as

$$F = 4\{(f_Y + \Delta f'_Y) \pm xf_C\} + 4i\Delta f''_Y. \qquad (1')$$

The observed and calculated structure factors are intercorrelated by

$$K|F_{obs}| = |F| \exp\left\{-B\left(\frac{\sin\theta}{\lambda}\right)^2\right\} = |F_{calc}|, \qquad (2')$$

where K is the scale factor as defined in Eq. (2) in Ch. IV.A. Note that the absolute value, $|F_{calc}|$, is employed in Eq. (2') rather than F_{calc} as used in Eq. (2). The logarithmic conversion of Eq. (2') gives

$$\underline{\ell n}(|F|/|F_{obs}|) = \underline{\ell n}\, K + B\left(\frac{\sin\theta}{\lambda}\right)^2. \qquad (3')$$

Based on Eq. (3'), the least-squares refinement was carried out for determining the best values for K and B at various carbon-occupancy parameters x.

The R_2 curves as a function of x with the dispersion correction are very much similar to those without the dispersion correction (see Fig. 1 of Ch. V.A). In the LOW ANGLE case, the R_2 curve gives a minimum value of 0.066% at x = 0.44 with B = 1.43 Å^2. The values obtained without the dispersion correction are R_2 = 0.072%, x = 0.48, and B = 1.67 Å^2. In the HIGH ANGLE case, the R_2 curve gives a minimum value of 0.22% at x = 0.44 with B = 1.74 Å^2. The values obtained without the dispersion correction are R_2 = 0.22%, x = 0.48, and B = 1.85 Å^2. The discrepancy factors are slightly in favor of the dispersion-corrected case. The nominal change in the scale factor manifests itself in a small difference in the x values. The change in the temperature factor is not appreciably large either.

The best set of parameters thus obtained are x = 0.44, leading to the formula $YC_{0.44}$ and B = 1.74 Å^2. The final values of $|F_{calc}|$ and $|F_{obs}|$ are listed in Table I', where the data for the first six reflections were obtained using the best parameters for the LOW ANGLE case, and the remainder were computed using the HIGH ANGLE parameters.

TABLE I'. Observed and Calculated Structure Factors per Unit Cell for the Cubic $YC_{0.44}$ with the Dispersion Correction. Note that in $F_{calc} = A_{calc} + iB_{calc}$, B_{calc} is as large as 16.0 for all reflections.

Indices	$\|F_{calc}\|$ NaCl Model	$\|F_{calc}\|$ CaF_2 Model	$\|F_{obs}\|$	Indices	$\|F_{calc}\|$ NaCl Model	$\|F_{calc}\|$ CaF_2 Model	$\|F_{obs}\|$
111	104.0	110.4	103.9 ± 4.4	600	36.1	33.2	38.1 ± 1.9
200	110.4	99.0	115.1 ± 2.3	442	36.1	33.2	35.1 ± 1.0
220	91.2	91.2	89.0 ± 1.9	620	32.3	32.3	30.6 ± 1.2
311	74.0	77.3	74.0 ± 2.0	533	27.5	28.7	29.3 ± 1.0
222	77.7	71.4	75.2 ± 2.9	622	29.1	26.7	30.6 ± 0.8
400	68.2	68.2	70.6 ± 2.3	444	26.4	26.4	23.6 ± 0.9
331	54.3	56.6	56.1 ± 1.1	711	22.2	23.2	19.5 ± 0.7
420	57.2	52.7	55.2 ± 2.0	551	22.2	23.2	21.8 ± 0.6
422	50.4	50.4	53.4 ± 1.2	640	23.7	21.7	25.2 ± 1.4
511	42.5	44.3	41.4 ± 1.0	642	21.5	21.5	22.7 ± 1.7
333	42.5	44.3	43.2 ± 2.2	553	18.1	19.0	20.0 ± 0.8
440	40.1	40.1	42.6 ± 1.0	820	15.9	14.5	18.0 ± 1.0
531	34.0	35.4	34.2 ± 0.5	644	15.9	14.5	16.4 ± 2.9

Our NaCl model (the octahedral case) gives the overall R_1 factor of 3.7% and the R_2 factor of 0.15%. For the CaF_2 model (the tetrahedral case),

we have $R_1 = 5.9\%$ and $R_2 = 0.46\%$. The difference here is not too large to endorse strongly the octahedral case. This situation is similar to the nondispersion case (see Ch. IV.B).

Subsequently, so as to establish the validity of the octahedral model, an analysis similar to the nondispersion case was carried out.

For reflections with h = odd, k = odd, and ℓ = odd, we have

$$\Sigma\{|F_{calc}(\text{octahedral})| - |F_{calc}(\text{tetrahedral})|\} = -108, \tag{6'}$$

where the summation was carried out on the all-odd index reflections in Table I', excluding the first six reflections. Now, the observed data give

$$\Sigma\{|F_{obs}| - |F_{calc}(\text{octahedral})|\} = 2 \simeq 0 \tag{7'}$$

and

$$\Sigma\{|F_{obs}| - |F_{calc}(\text{tetrahedral})|\} = -105 \simeq -108. \tag{8'}$$

Equations (6'), (7'), and (8') indicate almost complete agreement with the octahedral model.

For the reflection with (h = 4n+2, k = 4n+2, ℓ = 4n) and (h = 4n+2, k = 4n, ℓ = 4n) and their equivalent reflections, we obtain

$$\Sigma\{|F_{calc}(\text{octahedral})| - |F_{calc}(\text{tetrahedral})|\} = 133. \tag{9'}$$

This is compared with

$$\Sigma\{|F_{obs}| - |F_{calc}(\text{octahedral})|\} = -3 \simeq 0 \tag{10'}$$

and

$$\Sigma\{|F_{obs}| - |F_{calc}(\text{tetrahedral})|\} = 130 \simeq 133. \tag{11'}$$

Again, the octahedral case is strongly favored. The octahedral model is indistinguishable from the tetrahedral model for the reflection types (h = 4n, k = 4n, ℓ = 4n) and (h = 4n, k = 4n+2, ℓ = 4n+2). In this category,

$$\Sigma\{|F_{obs}| - |F_{calc}(\text{octahedral})|\} =$$

$$\Sigma\{|F_{obs}| - |F_{calc}(\text{tetrahedral})|\} = 25. \tag{12'}$$

The ideal value for Eq. (12') is zero, and the observed small value can well approximate this.

C. Trigonal Structure with Dispersion Correction

The final parameters in Case I in Ch. V.E were determined by the least-squares method with the dispersion terms taken into account. They are:

$$\Delta z = 0.0087 \pm 0.0003 \ (0.0085);$$

$$B_Y = 0.82 \pm 0.04 \ (0.98) \ \text{Å}^2;$$

$$B_C = 1.02 \pm 0.20 \ (1.05) \ \text{Å}^2;$$

$$K = 0.87 \pm 0.03 \ (0.93),$$

where the values in the parentheses were those determined without the dispersion correction. The important characteristic is that Δz is essentially unchanged. The differences in B_Y and K are significant, whereas that in B_C is insignificant. In Table III', $|F_{calc}|$ and $|F_{obs}|$ are listed using the newly obtained parameters. The discrepancy factors R_1 and R_2 are 5.1 and 0.47%, respectively. These values may be compared with the values 5.6 and 0.47% obtained without the dispersion correction. The dispersion correction did not vary the R-factors significantly.

TABLE III'. Observed and Calculated Structure Factors per Unit Cell of the Odd-ℓ Reflections of the Trigonal Y_2C with the Dispersion Correction. $F_{calc} = A_{calc} + iB_{calc}$. Note that relatively large B_{calc} values solely originated from the dispersion correction. Single and double asterisks are explained in Table III. Average standard deviation of the observed structure factor is about 5%.

Indices	A_{calc}	B_{calc}	$\|F_{calc}\|$	$\|F_{obs}\|$	Indices	A_{calc}	B_{calc}	$\|F_{calc}\|$	$\|F_{obs}\|$
003*	-47.70	3.90	47.9	**	0,0,21	59.64	16.56	61.9	67.9
101*	-2.37	1.29	2.7	<15.1	315	15.12	4.86	15.9	11.0
015	32.34	6.27	32.9	42.4	229	27.72	8.40	29.0	32.3
009*	59.49	10.80	60.5	**	137	-27.54	6.63	28.3	28.4
107	-60.93	8.52	61.5	65.1	0,2,19	-58.05	15.15	60.0	51.6
113*	-28.29	3.66	28.5	36.7	1,2,17	46.20	13.86	48.2	43.5
021*	0.57	1.20	1.3	<20.4	3,0,15	-47.82	12.63	49.5	55.0
0,1,11	-71.70	12.36	72.8	73.2	401*	0.33	0.93	1.0	<22.7
205	25.71	5.88	26.4	31.2	1,1,21	51.54	15.57	53.8	53.2
119	46.71	10.14	47.8	47.3	3,1,11	-36.06	9.60	37.3	39.1
027	-46.23	8.01	46.9	46.8	045*	12.93	4.59	13.7	<21.9
1,0,13	63.33	13.80	64.8	64.9	0,1,23	-57.66	15.99	59.8	57.7
0,0,15*	-77.82	15.24	79.3	96.3	407	-23.82	6.24	24.6	20.6
211*	0.81	1.14	1.4	<18.8	2,1,19	-50.07	14.25	52.1	49.3
2,0,11	-58.02	11.61	59.2	55.8	1,3,13	32.97	10.74	34.7	35.3
125	21.03	5.52	21.7	22.3	2,2,15	-41.22	11.85	42.9	41.7
217	-37.86	7.53	38.6	40.8	321*	0.24	0.90	0.9	<29.2
0,2,13	52.65	12.96	54.2	50.9	0,4,11	-31.47	9.03	32.7	28.5
303*	-18.09	3.24	18.4	<23.9	1,0,25	46.29	15.48	48.8	53.0
0,1,17	63.24	15.69	65.2	61.9	4,0,13	28.47	10.11	30.2	35.3
1,1,15	-65.10	14.31	66.6	66.4	413*	-7.11	2.52	7.5	<27.0
1,2,11	-48.93	10.89	50.1	51.1	3,1,17	34.62	12.24	36.7	39.4
309	32.61	8.94	33.8	33.6	3,0,21	38.52	13.71	40.9	48.3
1,0,19	-67.62	16.14	69.5	70.9	2,3,11	-27.30	8.46	28.6	27.5
2,1,13	44.61	12.18	46.2	45.7	419*	17.94	6.96	19.2	<26.1
223*	-15.42	3.03	15.7	<20.7	1,1,27	-41.31	14.13	43.7	47.9
2,0,17	53.76	14.76	55.8	56.0	0,1,29	34.92	13.80	37.5	45.3
131*	0.48	0.99	1.1	<25.1					

To distinguish Case I from other models, the analysis similar to the nondispersion case was also carried out. With the dispersion correction, the equations given in Ch. V.F are modified as follows:

$$(KF_{obs})^2 = |F_{calc}|^2$$

$$= \left[(-1)^{\frac{\ell-1}{2}} 6(f_Y + \Delta f'_Y) \sin(2\pi\ell\Delta z) \exp\left\{-B_Y\left(\frac{\sin\theta}{\lambda}\right)^2\right\} \right.$$

$$\left. - 3f_C \exp\left\{-B_C\left(\frac{\sin\theta}{\lambda}\right)^2\right\} \right]^2$$

$$+ \left[(-1)^{\frac{\ell-1}{2}} 6\Delta f''_Y \sin(2\pi\ell\Delta z) \exp\left\{-B_Y\left(\frac{\sin\theta}{\lambda}\right)^2\right\} \right]^2 . \quad (29')$$

The above equation is rearranged to

$$\sqrt{(KF_{obs})^2 - \left[6\Delta f''_Y \sin(2\pi\ell\Delta z) \exp\left\{-B_Y\left(\frac{\sin\theta}{\lambda}\right)^2\right\}\right]^2} \Big/ \left[6(f_Y + \Delta f'_Y) \exp\left\{-B_Y\left(\frac{\sin\theta}{\lambda}\right)^2\right\}\right]$$

$$= \left| \sin(2\pi\ell\Delta z) + (-1)^{\frac{\ell+1}{2}} \frac{Z_C \hat{f}_C}{2Z_Y \hat{f}'_Y} \exp\left\{-(B_C - B_Y)\left(\frac{\sin\theta}{\lambda}\right)^2\right\} \right| \quad (30')$$

$$= \begin{cases} \sin(2\pi\ell\Delta z) - \frac{1}{13}\frac{\hat{f}_C}{\hat{f}'_Y} & (\ell = 4n+1), \\ \sin(2\pi\ell\Delta z) + \frac{1}{13}\frac{\hat{f}_C}{\hat{f}'_Y} & (\ell = 4n-1), \end{cases} \quad (31')$$

where $\hat{f}'_Y = \hat{f}_Y + (\Delta f'_Y / Z_Y)$ and in deriving Eq. (31') from Eq. (30'), $B_C = B_Y$ was assumed. Averaging over a given ℓ leads to the equation

$$\left\langle \frac{\sqrt{(KF_{obs})^2 - \left[6\Delta f''_Y \sin(2\pi\ell\Delta z) \exp\left\{-B_Y\left(\frac{\sin\theta}{\lambda}\right)^2\right\}\right]^2}}{6(f_Y + \Delta f'_Y) \exp\left\{-B_Y\left(\frac{\sin\theta}{\lambda}\right)^2\right\}} \right\rangle_\ell = \begin{cases} \sin(2\pi\ell\Delta z) - \frac{1}{13}\alpha' & (\ell = 4n+1), \\ \sin(2\pi\ell\Delta z) + \frac{1}{13}\alpha' & (\ell = 4n-1), \end{cases}$$

(32')

where $\alpha' = \hat{f}_C/\hat{f}_Y$. The result based on Eq. (32') is illustrated in Fig. 11'. The experimental points for $\ell = 4n - 1$ lie consistently above the solid line representing $\sin(2\pi\ell\Delta\underline{z})$, and those for $\ell = 4n + 1$ lie below the solid line. The observed magnitude of these deviations gave approximately $\alpha' = 0.62$, which is in good agreement with the calculated mean value, $\alpha' = 0.68$.

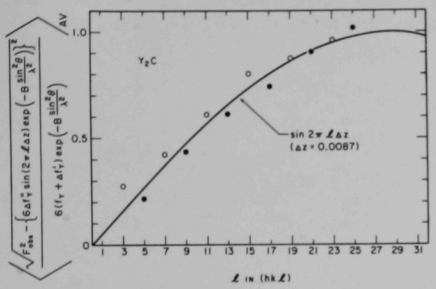

Fig. 11'

The Dispersion-corrected Diagram Corresponding to the Nondispersion Case Given in Fig. 11. Note that the distribution of the experimental points is almost identical to that given in Fig. 11. This implies that the dispersion correction does not alter the conclusions obtained without the dispersion correction.

121-4099

To recapitulate, the structural data obtained with and without the dispersion correction are tabulated in "Résumé of Dispersion Correction."

Résumé of Dispersion Correction

	YC_x (cubic)		Y_2C (trigonal)	
	Without Dispersion x = 0.48	With Dispersion x = 0.44	Without Dispersion	With Dispersion
Molecular Weight	94.69	94.20	189.9	No Change
Density (g/cm^3)	4.700	4.676	4.650	No Change
Coordinate of Y	4(a)	No Change	0.2585 ± 0.0003	0.2587 ± 0.0003
Interatomic Distance Y - C(Å)	2.558 ± 0.001	No Change	2.483 ± 0.003	2.486 ± 0.003
Interatomic Distance Y - Y(Å)	3.617 ± 0.002	No Change	3.402 ± 0.007 3.617 ± 0.002 3.904 ± 0.008	3.397 ± 0.007 3.617 ± 0.002 3.910 ± 0.008
Temperature Factor Coefficient of Y($Å^2$)	1.85 ± 0.08	1.74 ± 0.08	0.98 ± 0.04	0.82 ± 0.04
Temperature Factor Coefficient of C($Å^2$)	1.85 ± 0.008	1.74 ± 0.20	1.05 ± 0.20	1.02 ± 0.20
Mean Debye Temperature Θ (°K)	170 ± 5	173 ± 5	233 ± 6	274 ± 6

REFERENCES FOR NOTE ADDED IN PROOF

Templeton, D. H., *X-ray Dispersion Effects in Crystal-structure Determinations*, Acta Cryst. *8*, 842 (1955).

Cromer, D. T., *Anomalous Dispersion Correction Computed for Self-consistent Field Relativistic Dirac-Slater Functions*, Acta Cryst. *18*, 17 (1965).